STUDY AND ANALYSIS OF DISPERSION, EFFECTIVE AREA AND NONLINEAR PROPERTIES OF PHOTONIC CRYSTAL FIBER (PCF) AT DIFFERENT DOPING CONCENTRATION

A thesis submitted in partial fulfillment of the requirement for the degree of

Bachelor of Science
in
Electrical Electronic and communication Engineering

Submitted by

Anika Tahsin Haque	**Student ID:201116014**
Md. Al-Mamun Sabuz	**Student ID:201114046**
Mahmudul Hasan Shimanto	**Student ID:201116062**

Under the Supervision of

Group Captain Md. Afzal Hossain,psc

Department of Electrical, Electronic and Communication Engineering
Military Institute of Science and Technology (MIST)

2014

CERTIFICATION

This thesis paper titled **"Study and analysis of Dispersion, Effective Area and Nonlinear Properties of Photonic Crystal Fiber (PCF) at Different Doping Concentration"** is submitted by the group as mentioned below has been accepted as satisfactory and met the required standard in partial fulfillment of the degree of B Sc in Electrical Electronic and Communication Engineering on December 2014.

Group Members:

Anika Tahsin Haque

Md. Al-Mamun Sabuz

Mahmudul Hasan Shimanto

SUPERVISOR:

Group Captain Md. Afzal Hossain,psc

Department Head
Department of Computer Science and Engineering (CSE).
Military Institute of Science and Technology (MIST).

DECLERATION

It is hereby declared that the work presented in the thesis titled "**Study and Analysis of Dispersion, Effective Area and Nonlinear Properties of Photonic Crystal Fiber (PCF) at Different Doping Concentration**" is an outcome of the study carried out by the author under the supervision of Group Capt. Md. Afzal Hossain. It is also declared that neither this thesis paper nor any part therefore has been submitted anywhere else for the award of any degree, diploma or other qualifications.

AUTHORS:

Anika Tahsin Haque
Student ID:201116014

Md. Al-Mamun Sabuz
Student ID:201116046

Mahmudul Hasan Shimanto
Student ID:201116062

ABSTRACT

Intriguing design of Photonic Crystal Fiber (PCF) with nearly zero dispersion at operating wavelength with high nonlinear coefficient has been exploited. Several optical materials including SiO_2, GeO_2 doped silica and pure Si has been studied for optimizing a structure for a certain range of operating wavelengths. Design and optical characteristics of defected GeO2 doped SiO2 square core with regular hexagonal air hole cladding have been studied extensively. Modal analysis of the proposed geometries has been performed for a wide range of wavelengths including visible range (400 -700 nm), short-wavelength infrared band (1.4-3 μm) and mid-wavelength infrared band (3-8 μm). A good number of defected core structure such as ellipse, square and some other irregular structures constructed from Bezier curves have also been investigated to achieve nearly zero dispersion. Achieving smaller effective mode area is an important feature of our proposed structure. High nonlinear gain can be mentioned as the eligibility of the proposed fiber as a powerful candidate of Super Continuum Generation (SCG), Four Wave Mixing (FWM) and Polarization effect of PCF. In this thesis, different properties of defected GeO2 doped SiO2 square core like dispersion, effective mode area, nonlinear parameter etc. are investigated numerically using Full Vector Finite Element method(FEM). Several challenging issues in the field of nonlinear photonics have been identified which will help also to optimize an optical waveguide for nonlinear applications from different perspectives.

ACKNOWLEDGEMENT

We would like to express our sincere gratitude to our thesis supervisor Group Capt. Md. Afzal Hossain Senior Instructor and Head of the Department, Department of Computer Science and Engineering (CSE). We would like to express our heartfelt thanks gratefulness for his instructions, continuous encouragement, valuable discussions and careful review during the period of this research. His keen sight and wealth of farsighted advice and supervision have always provided us the precise guiding frameworks of this research. We have learned many valuable lessons and concepts of the Photonic Crystal Fiber (PCF) from him, which we have utilized to develop our abilities to work innovatively and to boost our knowledge. His constant encouragement gave us the confidence to carry out our work. We would also like to express our profound thanks and gratitude to all personalities our department of EECE for providing us with all out support during our thesis work.

Finally of course, we are grateful to our parents for their patience, love and endless prayers. Without their prayer this work would never have come into existence.

Dhaka

December 2014

Anika Thasin Haque

Md. Al-Mamun Sabuz

Mahmudul Hasan Shimanto

Content page

LIST OF FIGURE

LIST OF TABLE

LIST OF ABBREVIATIONS

PCF : Photonic Crystal Fiber

TIR : Total Internal Reflection

M-TIR : Modified Total Internal Reflection

MOF : Micro-structured Optical Fiber

PBG : Photonic Band Gap

ESM : Endlessly Single Mode

SCG : Super Continuum Generation

OSA : Optical Spectrum Analyzer

OCT : Optical Coherence Tomography

SCF : Suspended Core Fiber

CMC : Computer Numerical Control

FEM : Finite Element Method

PML : Perfectly Matched Layer

GVD : Group Velocity Dispersion

ZWD : Zero Wavelength Dispersion

WDM : Wavelength Division Multiplexing

DFB : Distributed Feedback

TOD : Third Order Dispersion

FWM : Four Wave Mixing

SPM : Self Phase Modulation

XPM : Cross Phase Modulation

DCF : Dispersion Compensating Fiber

DSF : Dispersion Shifted Fiber

LIST OF SYMBOLS

n : Refractive Index

α : Attenuation Constant

β : Propagation Constant

γ : Nonlinear Parameter

D : Dispersion

D_M : Material Dispersion

D_W : Waveguide Dispersion

Λ : Lattice Constant

d : Diameter of Air-Hole

ω : Angular Frequency

λ : Wavelength

Dedicated to Our Loving Parents

Chapter 1

Introduction

The idea of photonic crystals originated in 1987 from work in the field of the strong localization of light and in the inhibition of spontaneous emission. It was subsequently shown that in periodic arrangements of ideally lossless dielectrics, the propagation of light can be totally suppressed at certain wavelengths, regardless of propagation direction and polarization. This inhibition does not result from absorption but rather from the periodicity of the arrangement. The density of possible states for the light vanishes, so that even spontaneous emission becomes impossible. Such periodic arrangements of dielectrics have been called photonic crystals. The first fiber with a photonic crystal structure was reported by Philip St. J. Russell in 1995. Even if it was a very interesting research development, the first PCF did not have a hollow core, as shown in Fig. 1.1, and, consequently, it did not rely on a photonic band-gap for optical confinement [1].

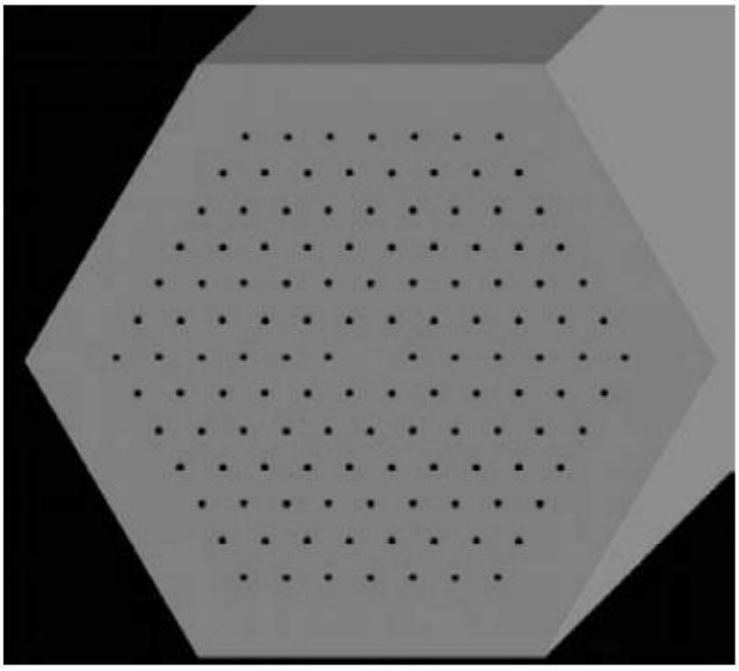

Fig 1. 1 Schematic of the cross-section of the first solid-core photonic crystal fiber, with air-hole diameter of 300 nm and hole-to-hole spacing of 2.3µm.

PCFs guides light by two mechanisms. One is the modified total internal reflection that utilizes its micro-structured cladding arrangement and solid core [2] and the other is photonic band gap mechanism in PCFs having hollow cores [3]. Optical fibers have a very broad range of application, where they serve many purposes, such as simply transporting light from source to some other device transmitting optically encoded data, sensing temperature or strain

in some environment, generating and amplifying laser light. These properties can be more easily achieved in PCFs as these fibers offer many degrees of freedom in their design than those of conventional optical fibers. Photonic Crystal Fibers (PCF) is a variant of the micro structured fibers with superior control of guiding properties. Such a vital photonic component has versatile applications in optical communications ranging from nonlinear optical signal processing to high power fiber amplifiers [4].

In this chapter, we have given a brief description of the basic principles of PCFs and their classifications. We have conducted a preliminary study of the improvement of PCF over conventional step index fibers. Besides, we have highlighted on their applications and state-of-the-art fabrication technologies. Finally we have investigated dispersion flattened and dispersion compensating fiber with small effective area and high non linearity parameters.

1.1 Basic Principles of PCF

In micro-structured fibers, the narrow silica core is surrounded by a silica cladding with embedded air holes. For this reason, such fibers are also known as "holey" fibers. For historical reasons, they are also referred to as the photonic crystal fibers (PCFs). In fact, such a fiber was first developed in 1996 in the form of a photonic-crystal cladding with a periodic array of air holes. It was realized later that the periodic nature of air holes is not critical for silica-core fibers as long as the cladding has multiple air holes that effectively reduce its refractive index below that of the silica core. In this case, light is guided by the total internal reflection, and the air holes are used to reduce the index of the cladding region. The periodic nature of the air holes become important in the so-called photonic band gap fibers in which the optical mode is confined to the core by periodic variations of the refractive index within the cladding. The core of such fibers often contains air to which light is confined by the photonic band gap. Such true PCFs can act as a highly nonlinear medium if air is replaced with a suitable gas or liquid.

1.1.1 One-Dimensional Photonic Crystals: Bragg Mirrors

The simplest device using the principles of photonic crystals is the one-dimensional photonic crystal, well known under the name of the Bragg mirror or the multilayer reflector. It consists of a periodic stack of two alternating dielectric layers. Light propagating in a direction normal to the layers undergoes successive reflection and transmission at each interface between adjacent layers. With an appropriate choice of layer thickness and refractive indices, waves reflected from each interface are in phase, whereas transmitted waves are out of phase. In that case, the transmitted wave components cancel each other out, and only the interference of the reflected components is constructive: the light is totally reflected.

1.1.2 Two and Three Dimensional Photonic Crystals

Photonic crystals with two- or three-dimensional periodicity can be seen as a generalization of Bragg mirrors. The simple approach using reflection and transmission matrices cannot be applied analytically here, and this is probably why their properties were discovered relatively recently .The point of using periodicities along two or three dimensions is to open up an Omni-directional band-gap: for the Bragg mirror, band-gaps at a given wavelength usually only exist for a finite range of angles of incidence, and propagation parallel to the Bragg layers can never be inhibited. With photonic crystals having a two-dimensional periodic arrangement of parallel rods, band-gaps can exist for all directions of propagation in the plane of periodicity, and for photonic crystals with three-dimensional periodicity, propagation of light in all directions can be prohibited. When a band-gap exists, regardless of direction of propagation and polarization, one speaks of a total photonic band-gap.

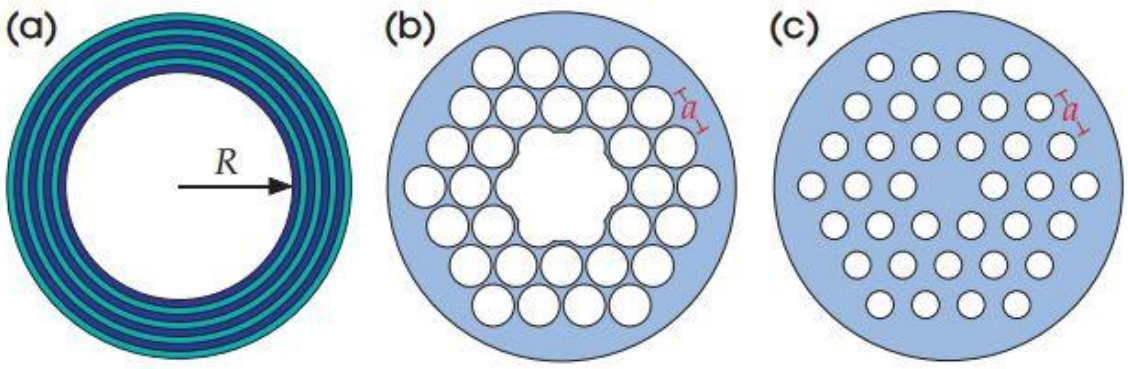

Fig 1. 2 Three examples of photonic crystal fibers. (a) Bragg fiber, with a one-dimensionally periodic cladding of concentric layer, (b) Two-dimensionally periodic structure (a tri-angular lattice of air holes, or "holey fiber") confining light in a hollow core

1.1.3 Guiding Mechanism in Photonic Crystal Fiber

For frequencies within a total photonic band-gap, no propagation is allowed in an infinite photonic crystal. If a defect is introduced in the infinite lattice, localized defect states for isolated frequencies within the band-gap can emerge. For three-dimensional photonic crystal lattices, this can be a single point defect: in that case light emitted from the defect will remain confined in the vicinity of the defect. It could also be a linear defect, in which case light remains in the locality of the defect but can propagate along it. Another way of looking at defect states is to consider the photonic crystal to be a perfect mirror in a certain frequency range. If one drills a hole all the way through the photonic crystal, light injected into the hole will be reflected at the borders of the hole and will propagate within it, in a similar way to light propagation in an optical fiber.

There is much very different geometry that allows guidance of light in micro-structured optical fibers, of which we will discuss the main below. A meaningful distinction to be made is between fibers in which light is guided in a core that has a refractive index lower than that of the photonic crystal in the cladding (for example hollow-core fibers), and fibers which have a core with refractive index higher than that found in the cladding (for example fibers with a solid core surrounded by holes)

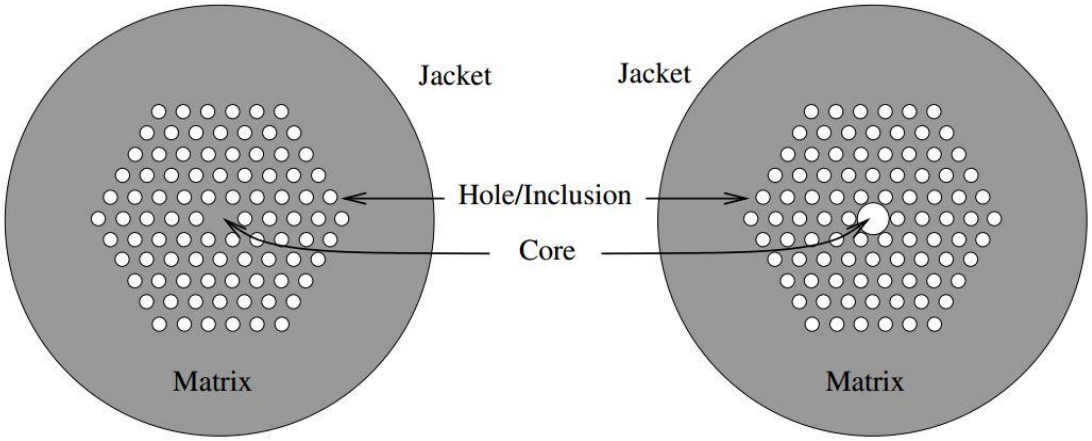

Fig 1. 3 Schematic representation of the cross section of a typical high-index, solid core MOF (left) and low-index, hollow-core MOF (right) with holes on a triangular lattice and a single central core.

In order to form a guide mode in an optical fiber, it is necessary to introduce light into the core with a value of β that is the component of the propagation constant along the fiber axis, which cannot propagate in the cladding. The highest β value that can exist in an infinite homogeneous medium with refractive index n is, $\beta=nk$, k being the free space propagation constant. A two-dimensional photonic crystal fiber, like any other material, is characterized by a maximum value of β which can propagate. At particular wavelength, this corresponds to the fundamental mode of an infinite slab of the material, and this value β_{eff} defines the effective refractive index n_{eff} of the material in the way, $\beta_{eff}=n_{eff}k$.

1.1.4 Modified Total Internal Reflection

It is possible to use two-dimensional photonic crystals as a fiber cladding, by choosing a core material with a higher refractive index than the cladding effective index. An example of this kind of structures is the PCF with a silica solid core surrounded by photonic crystal cladding with a triangular lattice of air holes, shown in fig 1.4. These fibers, also known as index-guiding PCFs, guide light through a form of total internal reflection (TIR), called modified TIR. However, they have a number of properties which vary from those of conventional optical fibers.

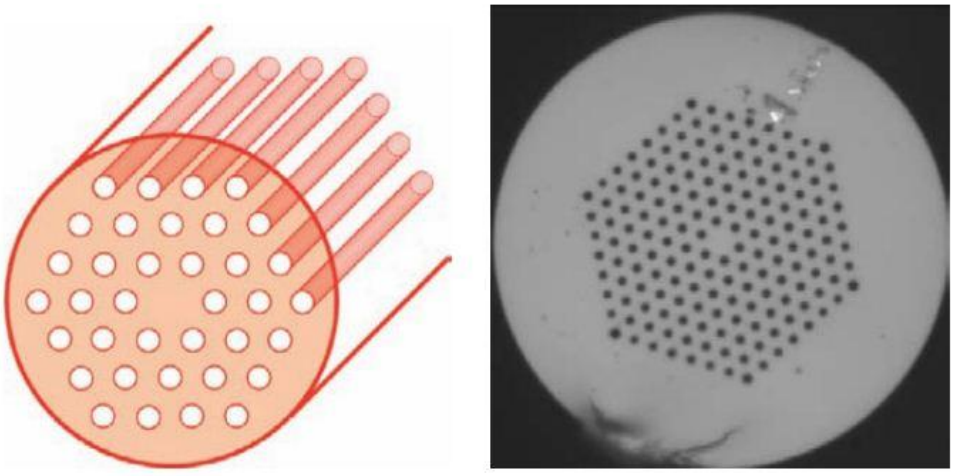

Fig 1. 4 (a) Schematic of a solid-core PCF with a triangular lattice of air-holes, which guides light for modified total internal reflection. (b) Micro-scope picture of a fabricated solid-core triangular PCF

1.1.5 Endlessly Single Mode Property

As already stated, the first solid-core PCF, shown in fig 1.1, which consisted of triangular lattice of air-holes with a diameter d of about 300 nm and a hole to hole spacing is 2.3um, did not ever seem to become multimode in the experiments, even for short wavelengths. In fact, the guided mode always had a single strong central lobe filling the core [3].

Russel has explained that this particular endlessly single-mode behavior can be understood by viewing the air-hole lattice as a modal filter or sieve [3]. Since light is evanescent in air, the air holes acts like strong barriers, so they are the "wire mesh" of the sieve. The field of the fundamental mode, which fits into the silica core with a sing lobe of diameter between zeros slightly equal to 2Λ, is the grain of rice which cannot escape through the wire mesh, being the silica gaps between the air holes belonging to the first ring around the core too narrow. On the contrary, the lobe dimensions for the higher order modes are smaller, so they can slip

between the gaps. When the ratio d/ʌ, that is the air filling fraction of the photonic crystal cladding, increases, successive higher order modes become trapped [3].

A proper geometry design of the fiber cross section thus guarantees that only the fundamental mode is guided. More detailed studies of the properties of triangular PCFs have shown that this occurs for d/ʌ <.4 [6]-[7].

By exploiting this property, it is possible to design very large mode are fibers, which can be successfully employed for high power delivery, amplifiers, and lasers. Moreover, by doping the core in order to slightly reduce its refractive index, light guiding can be turned off completely at wavelength shorter than a certain threshold value.

1.1.6 Photonic Band-gap Guidance

Optical fibers designs completely different from the traditional ones result from the fact that photonic crystal cladding have gaps in the ranges of the supported modal index β/k where there are no propagation modes. These are the PBGs of the crystal, which are similar to the two dimensional band-gaps which characterize planar light wave circuits, but in this case they have propagation with a non-zero value of β. It is important to underline that gaps can appear for values of modal index both greater and smaller than unity, enabling the formation of hollow core fibers with band-gap material as a cladding, as reported in fig 1.5(b). These fibers, which cannot be made using conventional optics, are related to Braggs fibers, since they do not rely on TIR to guide light. In fact, in order to guide light by TIR, it is necessary a lower index cladding material surrounding the core, but there are no suitable low loss material with a refractive index lower than air at optical frequencies [2]. The first PCF which exploited the PBG effect to guide light was reported in 1998 [3]-[8], and it is shown in fig 1.4. Notice that its core is formed by an additional air hole in a honeycomb lattice. This PCF could only guide light in silica that is in the higher index material.

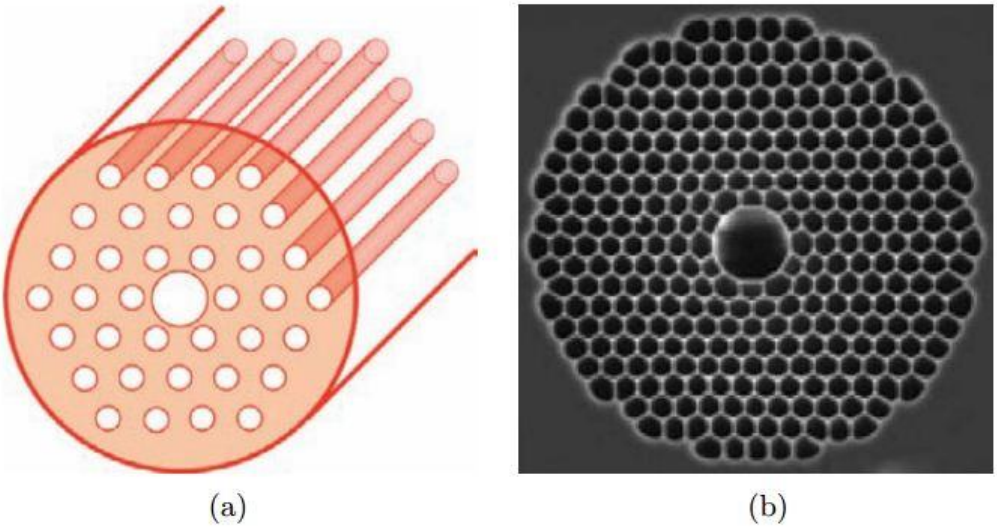

Fig 1. 5 (a) Schematic of a hollow-core PCF with a triangular lattice of air-holes, which guides light through the photonic band-gap effect. (b) Micro-scope picture of a fabricated hollow-core triangular PCF

Hollow core guidance had to wait until 1999, when the PCF fabrication technology had advanced to the point where larger air filling fractions, required achieving a PBG for air guiding, became possible [3]. Notice that is guided mode must have $\beta/k<1$, since this condition guarantees that light is free to propagate and form a mode within the hollow core, while being unable to escape into the cladding. The first hollow core PCF, reported in fig 1.5(b), had a simple triangular lattice of air holes, and the core was formed by removing seven capillaries in the center of the fiber cross section. By producing a relatively large core, the chances of finding a guided mode were improved. When white light is launched into the fiber core, colored modes are transmitted, thus indicating that light guiding exists only in restricted wavelength ranges, which coincide with the photonic band-gaps [3].

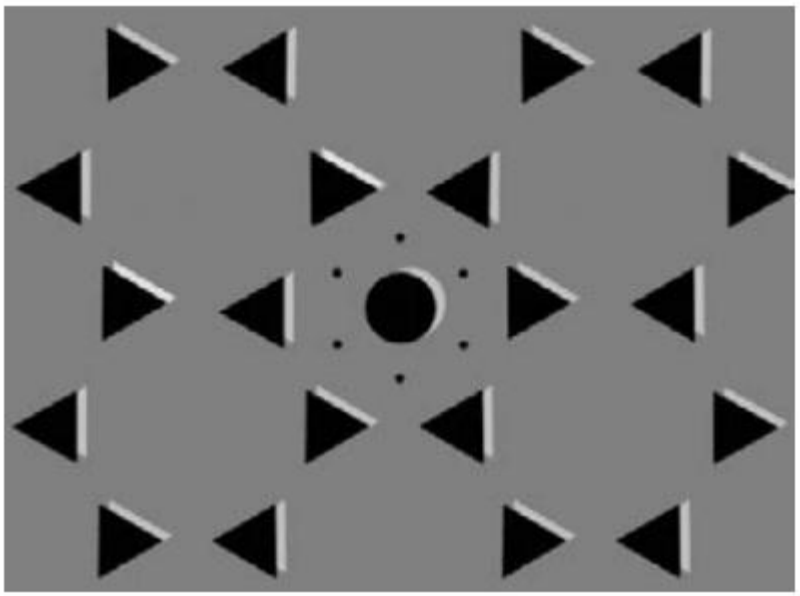

Fig 1. 6 Schematic of the cross-section of the first photonic band-gap PCF With a honeycomb air-hole lattice

1.1.7 Solid Core Fibers

Index guiding PCFs, with a solid glass region within a lattice of air holes, offer a lot of new opportunities not only for applications related to fundamental fibers optics. These opportunities are related to some special properties of the photonic crystal cladding, which are due to the large refractive index contrast and the two dimensional nature of the microstructure, thus affecting the birefringence, the dispersion, the smallest attainable core size, the number of guided modes and the numerical aperture and the birefringence.

1.1.8 Highly Birefringence Fibers

Birefringence fibers, where the two orthogonally polarized modes carried in a single mode fiber propagate at different rates, are used to maintain polarization states in optical devices and subsystems. The guided modes become birefringent if the core microstructure is deliberately made two fold symmetric, for example, by introducing capillaries with different wall thicknesses above and below the core. By slightly changing the air hole geometry, it is possible to produce levels of birefringence that exceed performance of conventional exceed the performance of conventional birefringent fiber by an order of magnitude. It is important to underline that, unlike traditional polarization maintaining fibers, such as bow tie, elliptical core or panda, which contain at least two different glasses, each one with a different thermal expansion coefficient, the birefringence obtainable with PCFs is highly insensitive to

temperature, which is an important feature in many applications. An example of the cross section of a highly birefringent PCF is reported in fig 1.7.

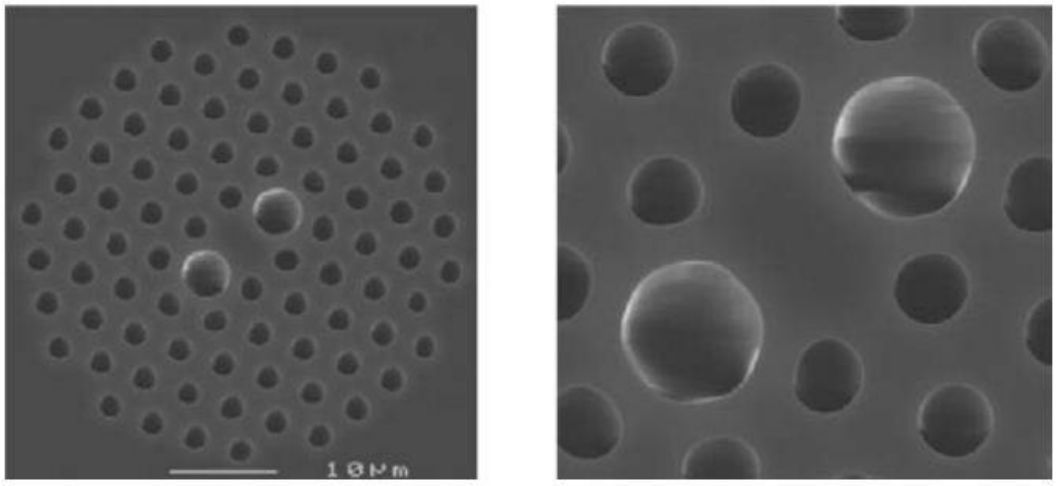

Fig 1. 7 Microscope picture of (a) the cross-section and (b) the core region of a highly birefringent triangular PCF

1.1.9 Dispersion Tailoring

The tendency for different light wavelengths to travel at different speeds is a crucial factor in the telecommunication system design. A sequence of short light pulses carries the digitized information. Each of these is formed from a spread of wavelengths and as a result of chromatic dispersion, it broadens as it travels, thus obscuring the signal. The magnitude of the dispersion changes with the wavelength passing through zero at 1.3 um in unprecedented freedom. In fact, due to the high refractive index difference between silica and air, and to the flexibility of changing air hole sizes and patterns, a much broader range of dispersion behaviors can be obtained with PCFs that with standard fibers. For example, as the air holes get larger, the PCF core becomes more and more isolated, until it resembles an isolated strand of silica glass suspended by six thin webs of glass, as it is shown in fig 1.8 if the whole structure s made very small, the zero dispersion wavelength can be shifted to the visible, since the group velocity dispersion is radically affected by pure waveguide dispersion. On the contrary, very flat dispersion curves can be obtained in certain wavelength ranges in PCFs with small air holes that is with low air filling fraction. As an example, a dispersion flattened triangular PCF with seven air hole rings, characterized by Λ=2.5 um, and d=0.5 um, has been presented in [9].

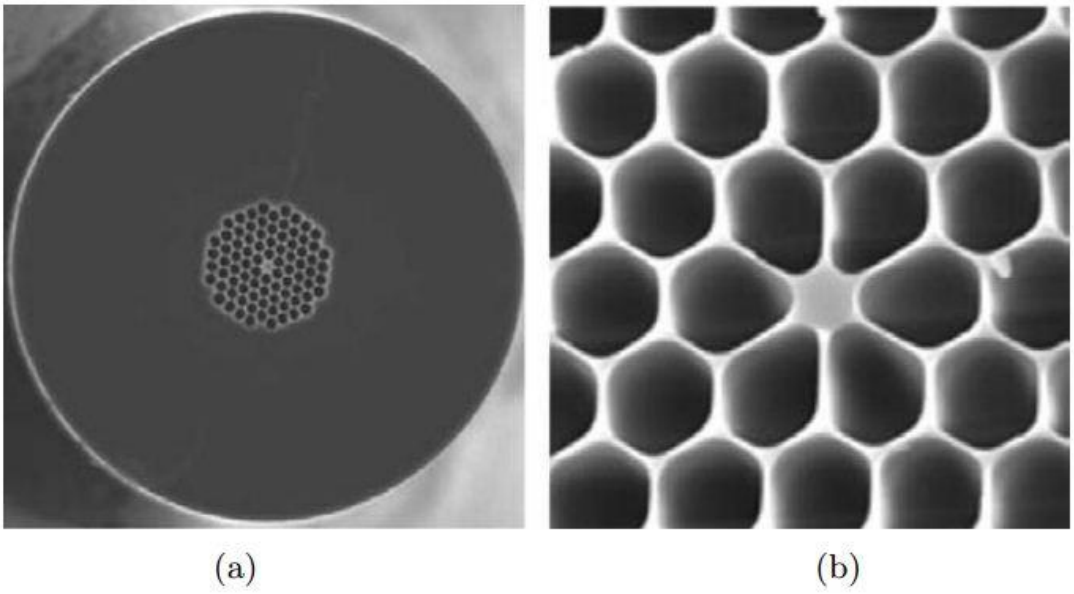

Fig 1. 8 Microscope picture of (a) the cross-section and (b) the core region of a highly nonlinear PCF, characterized by a small-silica core and large air-holes, with zero-dispersion wavelength.

1.2 Classifications of PCF

In this section, we have highlighted on different variants of photonic crystal cladding fabricated so far. The objective of this section is to make familiarize with the versatility of in photonic crystal fiber technology and maturity its fabrication technology. In Fig. 1.6 representative sketches of different types of PCFs are provided. However, design of a PCF is highly dependent on its application and choice of certain materials in different bands of wavelengths. We have considered two distinct principles of propagation for analyzing several linear and nonlinear properties of PCF according to [10]. They are:

1.2.1 Positive Core-Cladding Index Difference:

This type of PCF may be defined as one where the mean cladding refractive index in a certain wavelength is lower than the core index. As discussed earlier, these PCFs will generally maintain TIR-guided modes which are also verified experimentally. Detailed method of analysis will be provided in the methodology chapter. Some of the important applications under this principle are:

Controlling the Number of Modes:

Controlling the number of modes in a waveguide can be more flexible through the design of photonic crystal cladding. A fiber can be endlessly single mode (ESM) at all operating wavelengths if carefully designed.

Ultra-Large-Area Single Mode:

This condition is important when a PCF is operated under high power to eliminate undesirable nonlinear effect.

Fibers with Multiple Core:

These fibers find applications in curvature sensing, cladding-pumped lasers, two-photon fluorescence etc.

Nanoweb Fibers:

It does not have a deliberately introduced core but instead relies on a gentle thickness gradient to confine the light. The extremely low loss (0.4dB/m) in what is essentially a planar glass waveguide with very strong waveguide dispersion makes this an interesting structure for experiments in spatial solitons and nonlinear optics.

1.2.2 Negative Core-Cladding Index Difference:

Since TIR is not possible here, low loss wave guiding is only possible if PBG exists. Some of the major variants under these principles are discussed below:

Hollow core Photonic Band Gap Fiber:

A special class of PBG guiding fibers is the hollow core fibers, where the field is confined to an air-filled core. Like other PBG fibers, air-core fibers only guide light in a limited spectral region. For fibers guiding around 1550nm, a typical bandwidth is ~200nm. Outside this region, the fiber core is anti-guiding. Guiding light in a hollow core holds many promising applications like high power delivery without the risk of fiber damage, gas sensors or extreme low loss guidance in vacuum. Furthermore, this class of fiber has other spectacular properties not found in any other fiber type. They are almost insensitive to bending (even at very small bending radii) and they have dramatically reduced sensitivity to Kerr effect (>50), temperature transients (~6.5), and Faraday Effect (>10). Also, extreme dispersion properties, such as anomalous dispersion values in the thousands of ps/nm/km regime are easily obtained. Due to a negligible contribution from the core material (air), the total dispersion of PBG fibers is to a high degree dominated by waveguide dispersion.

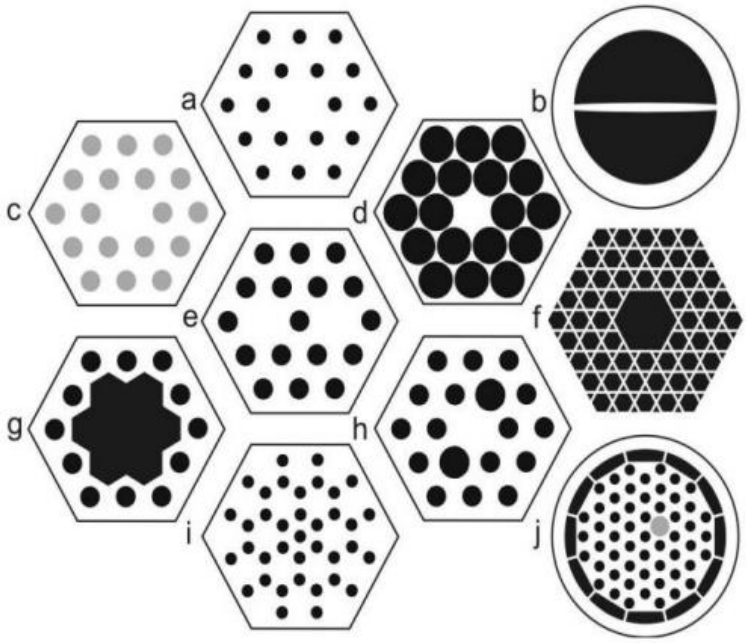

Fig 1. 9 Representative sketches of different types of PCF. The black regions are hollow, the white regions are pure glass, and the gray regions are doped glass. (a) ESM solid-core PCF. (b) Nanoweb fiber (not a PCF). (c) All-solid-glass PCF with raised-index doped glass strands (colored gray) in the cladding. (d) SC PCF (with high air-filling fraction and small core). (e) Dual-core PCF. (f) Kagomé hollow-core PCF. (g) Seven-cell hollow-core PCF. (h) Birefringent PCF. (i) Carbon-ring structure for PBG guidance. (j) Double-clad PCF with off-set doped lasing core and high numerical aperture inner cladding for pumping the photonic-crystal cladding is held in place by thin webs of glass [11].

Glass of Higher Refractive Index:

This kind of PBG fiber may have wider band gap than the low index contrast counterparts. Due to high index contrast, a vectorial method may be required to trace out the accurate band-gap region. This high index contrast condition may occur when longer operating wavelengths are concerned for several sensing applications. Like other PBG fibers, solid core PBG fibers only guide light in a limited spectral region. This filtering effect in combination with a rare earth doped core such as Yb makes lasing and amplification possible at new wavelengths with weak fiber gain. Also, the combination of a doped solid core PBG fiber and special dispersion properties provides a new route for the laser community.

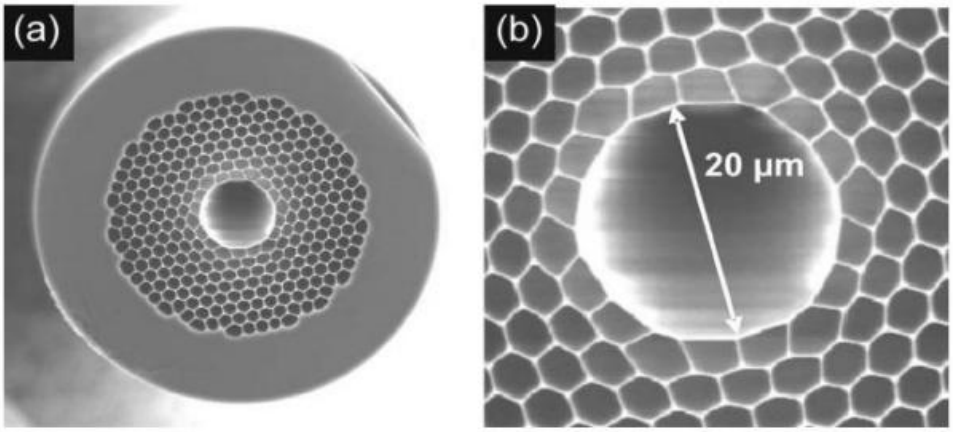

Fig 1. 10 (a) Example of a low-loss hollow-core PCF. The core diameter is 20.4 µm, and the attenuation in the best cases approaches 1 dB/km at 1550 nm wavelength. (b) Detail of the core region [11].

Surface States on Core–Cladding Boundary:

This phenomenon may occur in PBG fibers. In the Fig. 1.11, we have shown the formation of such states.

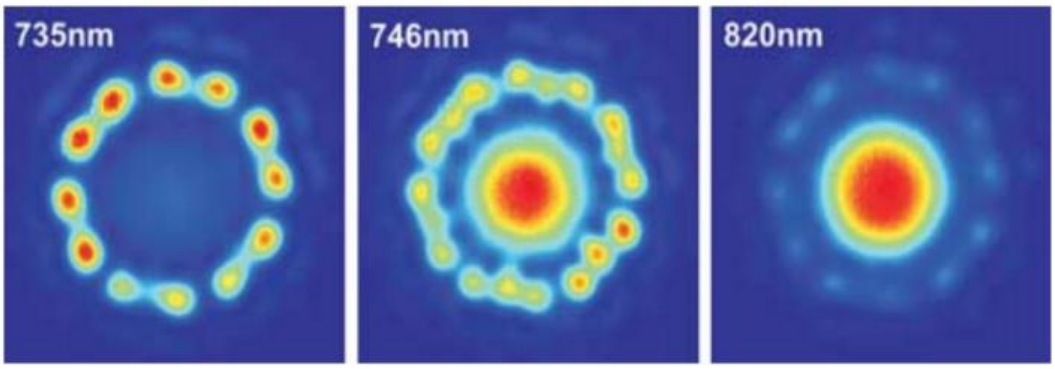

Fig 1. 11 Near-field end-face images of the light transmitted in hollow-core PCF designed for 800nm transmission. For light launched in the core mode, at 735 nm, a pure surface mode is transmitted, at 746 nm, a coupled surface-core mode is transmitted, and at 820 nm, a pure core mode is transmitted [11].

All-Solid Structure PBG Fiber:

In all-solid band gap guiding fibers, the core is made from low-index glass and is surrounded by an array of high-index glass strands. Since the mean core–cladding index contrast is negative, TIR cannot operate, and PBG effects are the only possible guidance mechanism. It is possible to achieve PBG guidance by this mechanism even at index contrasts of 1% with losses as low as 20 dB/km at 1550 nm. Apart from such classifications, PCFs can be identified distinctly based on their several properties like birefringence, dispersion and operating wavelengths. In our thesis, we have focused on design of PCFs with high nonlinear effect and better dispersion control mechanisms most importantly. We have also considered sub wavelength core diameter design favored by recent fabrication technology for exploiting nonlinear applications at a low threshold power.

1.3 Application of PCF

1.3.1 Photonic Crystal Fiber for Communication Applications

The rapid development of optical fiber communication has created a strong need for novel optical components that can handle functions such as dispersion compensation and wavelength division multiplexing. Photonic crystals offer many exciting opportunities for developing new optical components for optical communications. The crystal structures are very well known for their potentials for confining and guiding light in very small structures. Photonic crystals can also exhibit strong dispersion properties that may give rise to large group delay, strong chromatic dispersion, and significant polarization-dependent dispersion for pulse propagation. Therefore, photonic crystals offer exciting potentials for key enabling technologies in optical communication systems, such as delay elements, chromatic dispersion compensators, polarization mode dispersion mitigators, and wavelength add/drop filters. To realize the potentials of photonic crystals, it is critically important to understand how photonic crystal structures can be engineered to meet the stringent requirements of optical communications [12].

1.3.2 Photonic Crystal Fiber for Super-continuum Generation

Super-continuum generation (SCG) is a process where laser light is converted to light with a very broad spectral bandwidth (i.e., low temporal coherence), whereas the spatial coherence usually remains high. The spectral broadening is usually accomplished by propagating optical pulses through a strongly nonlinear device, such as an optical waveguide. The advent of a new class of optical waveguides in the form of the PCF in the late 1990s attracted widespread interest throughout the scientific community, and has led to a revolution in the generation of ultra-broadband high brightness spectra through SC generation [13]. It is mainly due to their unusual chromatic dispersion characteristics, which can allow a strong nonlinear interaction over a significant length of fiber. Even with fairly moderate input powers, very broad spectra are achieved. This leads to a kind of laser rainbow. In some cases, tapered fibers can also be

used. If we want to compare the laser sources with SC sources, the unique feature of lasers is that they are monochromatic – their output consists of just one wavelength. Another special property is that they are exceptionally bright when compared to thermal white light sources. A large amount of power is not only concentrated in a small spectral window but also can be focused tightly onto a small area. Despite their low brightness, white light sources have a wide range of applications, due to their broad and smooth spectrum and low temporal coherence. SC sources are a new type of light sources that provide a combination of these desirable features: high output power, a broad, flat spectrum, and a high degree of spatial coherence that allows tight focusing. When compared to a thermal (incandescent) fiber coupled source, the SC source covers a comparable spectral range, but is thousands of times brighter, providing a signal-to-noise advantage of 30-40 dB in many applications as shown in Fig 1.12.

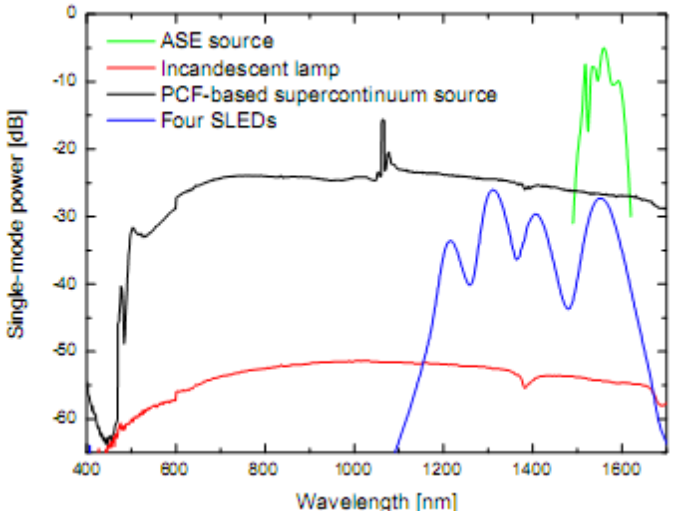

Fig 1. 12 Comparison of the power spectral density delivered into a single mode fiber for various broadband light sources.

A SC source typically consists of a pulsed laser and a nonlinear element, in which a combination of nonlinear effects broadens the narrowband laser radiation into a continuous spectrum without destroying the spatial coherence of the laser light. PCFs are uniquely suited as the nonlinear medium for such sources, offering high nonlinearity, suitable dispersion characteristics and ease of use. The experimental setup of the SCG in a PCF pumped by ultra-short pulses is illustrated in Fig. 1.13. The linearly polarized ultra-short pulses from a mode-locked laser first passed through a variable optical attenuator consisting of a half-wave plate, a polarization cube beam splitter and a neutral density filter. Then the laser pulses were coupled into the PCF using an objective lens. The far end of the cleaved fiber was inserted into an optical spectrum analyzer (OSA).

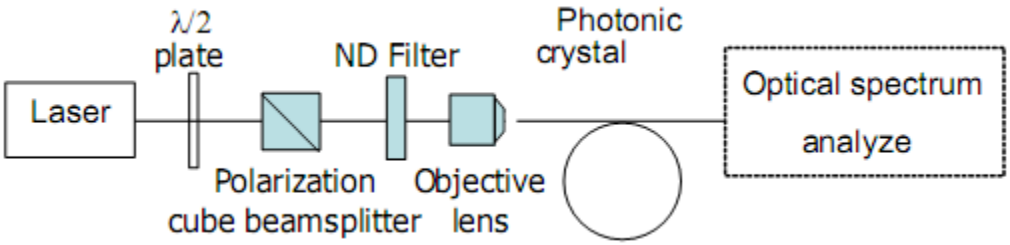

Fig 1. 13 Schematic drawing of the experimental setup for SCG in a photonic crystal fiber pumped with ultra-short laser pulses.

1.3.3 Photonic Crystal Fiber for Medical Applications

Optical coherence tomography (OCT) is a new technology for noninvasive cross-sectional imaging of tissue structure in biological system by directing a focused beam of light at the tissue to be image. The technique measures the optical pulse time delay and intensity of backscattered light using interferometry with broadband light sources [14]. OCT depends on optical ranging means distances are measured by shining a beam of light onto the object, then recording the optical pulse time delay of light. Different internal structures produce different time delays, and cross-sectional images of the structures can be generated by scanning the incident optical beam. The wavelength range of the OCT light source is spread from the 0.8 to 1.6$\mu m$and. This spectral region is of particular interest for OCT because it penetrates deeply into biological tissue and permits spectrally resolved imaging of water absorption bands. This can be achieved by super-continuum (SC) light using photonic crystal fibers.

1.3.4 Photonic Crystal Fiber for Sensing Technology

Suspended Core Fiber (SCF) has been widely used in different sensing applications from physical science to life science due to its some discernible properties concerning sensing applications. Recently, advanced DNA sensing, broadband chemical sensing, and various sensing application has been exploited with SCF [15]-[16].The air holes of SCF are infiltrated with sample materials and core fields interact with these materials evanescently. Large air hole of SCF helps in speeding up the filling process by sample materials through the air holes in sensing applications. High air filling fraction ensures higher interaction between evanescent field and sample materials. Moreover, broad spectral features have made SCF unparalleled in sensing applications. A typical setup for the sensing application is shown in the below Fig 1.14.

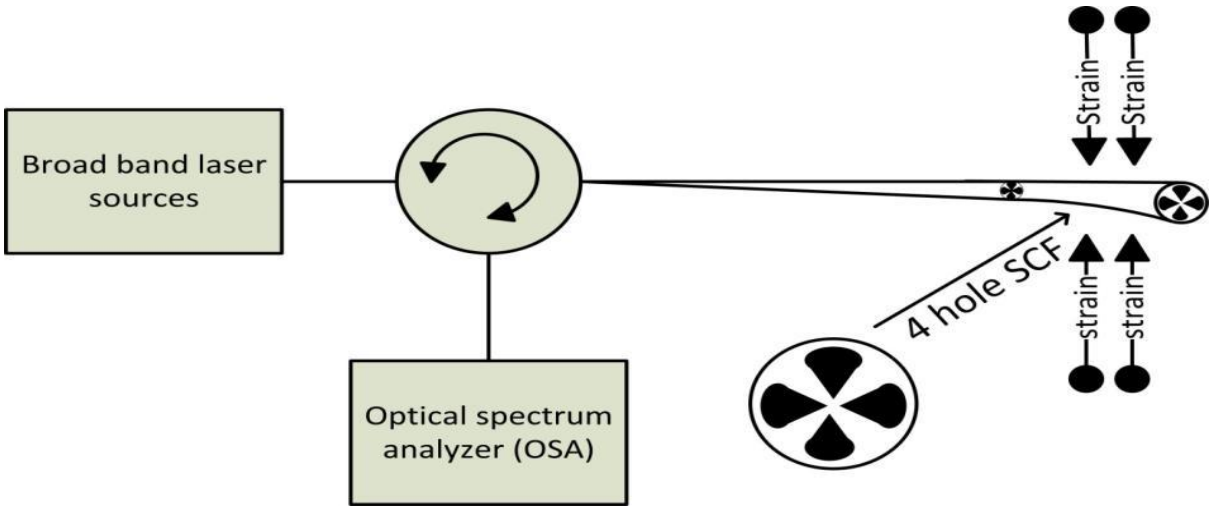

Fig 1. 14 Experimental setup for sensing with Suspended Core Fiber.

In the above setup tapered SCF can be used to couple with the standard single mode fiber like SMF-28. Broad band optical source is needed for SCF based applications. Ultra low core of SCF enhances fiber nonlinearity which can be exploited in super-continuum based sensor applications. Increased sensitivity of fiber can be ensured by enhancing the evanescent field which demands more research work in SCF based fiber sensor.

1.4 Fabrication Technology of PCFs

Micro-structured optical fibers (MOFs) contain an array of wavelength-scale air holes within the fiber cross-section, which allows a broad range of novel optical properties. PCFs are optical fibers that employ a micro structured arrangement of material in a background material of different refractive index. The background material is often undoped silica and a low index region is typically provided by air voids running along the length of the fiber [21].

PCFs may be divided into two categories, high index guiding fibers (holey fibers) and low index guiding fibers (photonic band-gap fibers). Similar to conventional fibers, high index fibers are guiding light in a solid core by the modified total internal reflection (M-TIR) principle. The total internal reflection is caused by the lower effective index in the micro structured air filled region.

Low index guiding fiber known as guide light by the photonic band-gap (PBG) effect. The light is confined to the low index core as the PBG effect makes propagation in the micro structured cladding region impossible.

Optical fibers in general are fabricated by a two-step process: fiber preform fabrication and fiber drawing. As opposed to preform fabrication for standard optical fibers where chemical processes such as chemical vapour deposition and polymerization are used, PCF technology requires more specific preform fabrication techniques influenced by the material and the structure of the desired fibers. In the fiber-drawing step a large-scale (structured or not) preform is reduced to fiber dimensions. This process is in principle similar in conventional and MOF technology. However, special considerations have to be made in the MOF case due

to the different structure geometries and the microscopic air holes of the fiber structure.

1.4.1 Stacking Fabrication Technique

Fabrication of PCF, like in conventional fiber fabrication, starts with a fiber perform in a fiber-drawing tower, an apparatus which is typically several meters high. The preform is a glass rod with a diameter between about 1 and 10 cm and roughly 1 m length. Along its axis, the preform contains a region with increased refractive index, which will form the fiber core. When the preform is heated close to the melting point in a furnace at the top of the drawing tower, a thin fiber can be pulled out of the bottom of the preform. The fiber from a single preform can be many kilometers long. During the pulling process, the fiber diameter is held constant by automatically adjusting the pulling speed and possibly the furnace temperature with an automatic feedback system.

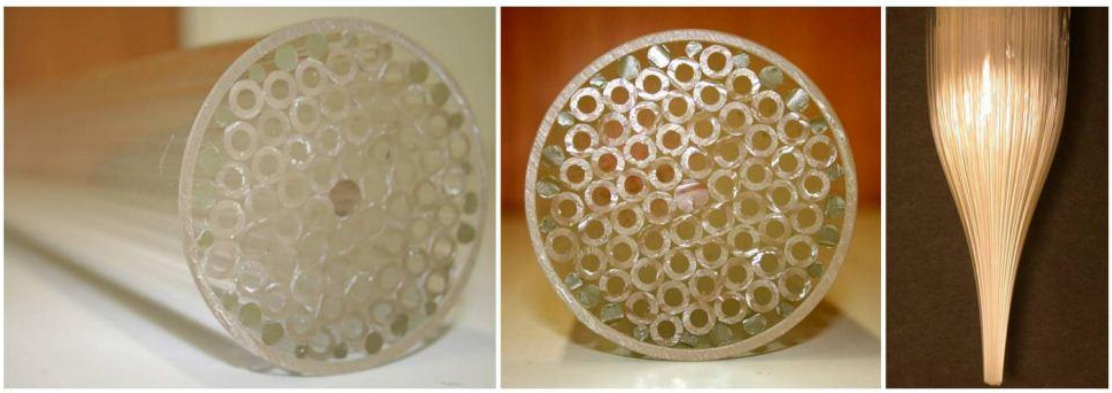

Fig 1. 15 Solid-core index-guiding photonic crystal fiber preforms fabricated by the stacking method. (Centre) Detail of the closely triangularly packed capillaries.

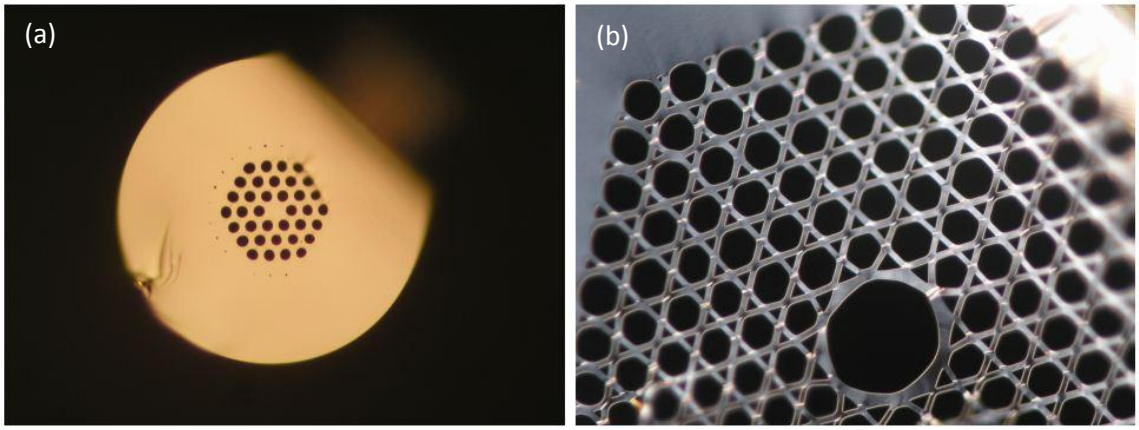

Fig 1. 16 Chalcogenide MOFs obtained with the stack and draw technique (a) Solid-core MOF with three rings of air holes (GaGeSbS glass). (b) Hollow-core MOF with six rings of air holes TAS glass.

Fiber pulling works quite well for the usual silica fibers, since silica a large range of temperatures in which the viscosity is in a suitable range. Other materials like fluoride fibers, have a much smaller temperature range suitable for pulling, and the method is accordingly more delicate.

Before the fiber is wound up, it usually receives a polymer coating for mechanical and chemical protection. Such coatings can consist of two or more different layers for optimum suppression of micro-bends. Typical coating materials used is acrylate, silicone and polyimide. Additional PVC or similar protective coatings can be made by extrusion after the drawing process. The final fibers are comparable to standard fiber in both robustness and physical dimensions and can be both striped and cleaved using standard tools. It is important to note that the stacking technique is limited in terms of different structure geometries. This method is practically limited to triangularly and square packed capillaries or simple radial geometry structures with a low number of capillary layers

In this section, we are reporting three novel fabrication technologies to realize more complex configurations of PCFs. In our thesis, we have characterized PCFs for a wide range of applications which cannot be fabricated by the conventional stack and draw technique mentioned earlier.

1.4.2 Drilling Technique

Drilling is the most widely used method for polymer MOF fabrication, due to the machine-friendly mechanical properties of polymers. Drilling preforms allows for rapid fabrication and indeed prototyping of new MOF designs, making this method

an ideal research manufacturing technique. This approach can readily produce structures that are difficult if not impossible to produce by capillary stacking

A diversity of complex preforms can be accurately made in an automated fashion by drilling with a computer numerical control (CNC) mill. Such designs can require several hundred closely spaced holes of different sizes to be drilled. The use of special coated drill bits allows quite deep holes to be produced while leaving the inside of the holes with an acceptable smooth finish. This is important since surface roughness will introduce an excess of scattering losses in the drawn fiber.

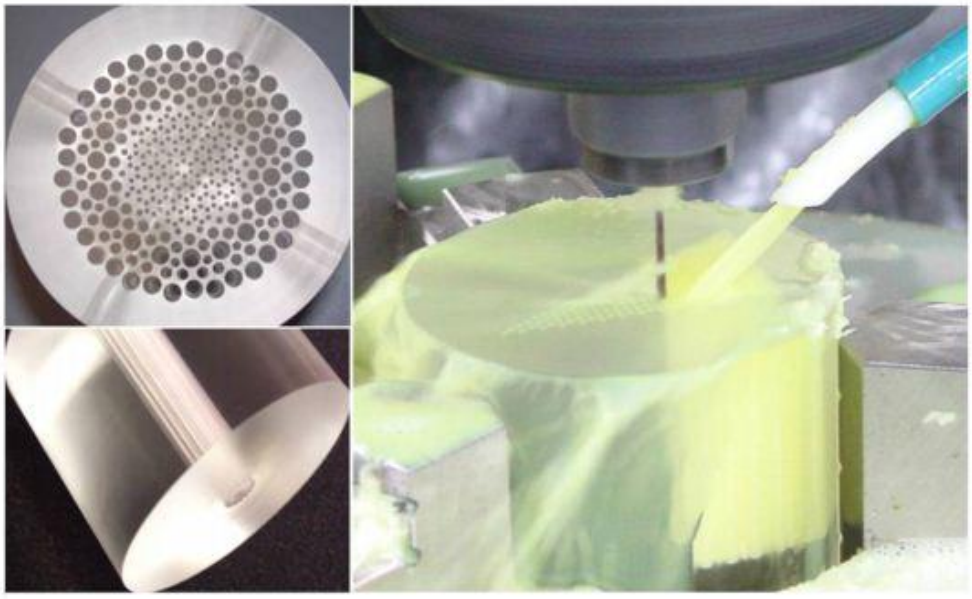

Fig 1. 17 Preform drilling technique for a polymer micro-structured fiber. (Right) CNC automated drilling machine during the process. (Top left) Detail of an extremely complex polymer PCF preform.

This drilling technique imposes a limitation on the length of the fabricated MOF preforms. The longest preform that has been drilled in polymer to date was 140 mm, and this was achieved by drilling to a 70mm depth with 2 mm drill bits from both ends of the preform. The produced preforms are usually short and fat. One consequence here is that to achieve desired hole or core dimensions generally requires a two-stage preform drawing process, where the intermediate cane from the first stage is sleeved within a tube before being drawn a second time. The short and fat preforms generally lead to a large amount of wasted material during the preform drawing process.

1.4.3 Extrusion and Casting Technique

Alternatives to drilling and stacking have been used for producing MOF preforms. These include extrusion and casting, each of which results in a monolithic preform in which the entire hole structure is created in a single- stage process

1.4.3.1 Extrusion Technique

The successful realization of a range of Micro structured optical fiber (MOF) depends on the use of complex air/glass structures within the fiber cross-section. Other techniques have been used to fabricate structured preforms. These techniques all have limitations in the number of transverse features, hole shapes and configurations that can be achieved. A promising alternative technique is billet extrusion, which has been shown to be a versatile, reproducible single-step approach to fabrication of soft glass and polymer preforms with up to 12 holes. Under high pressure and high temperature, the material flow can be extruded through a machined die so that a preform with the desired MOF structure can be fabricated. This technique is especially suitable for making glass preforms based on those glasses with a narrow temperature operating range (known as soft glasses) or glasses with a high tendency to crystallize [17].

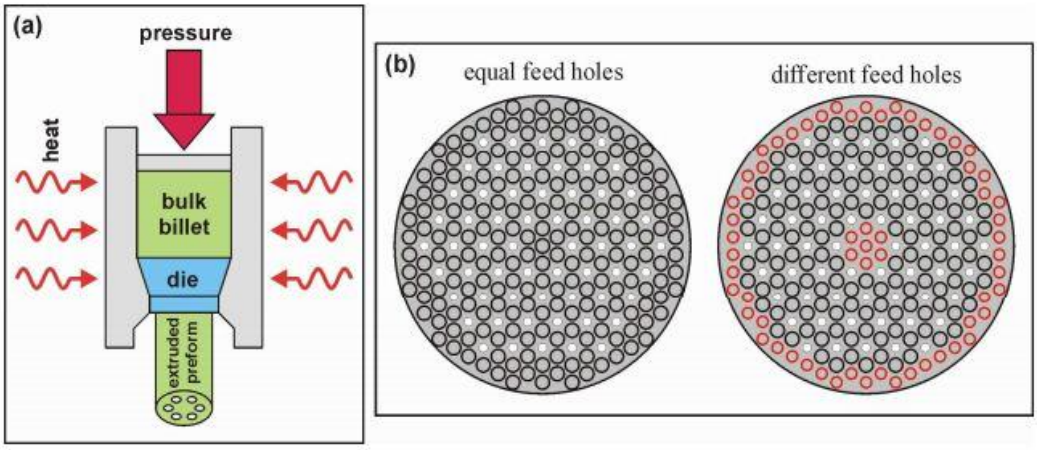

Fig 1. 18 (a) Sketch of extrusion process and (b) extrusion die concepts with equal and different size feed holes for a target preform structure having 60 holes (4 rings), white filled circles are blocking elements, and black and red circles are feed holes

In Fig 1.18, overall process has been shown. This new die design allows great flexibility in the selection of the size, shape and distribution of the feed holes, which provides control of the material flow through the die in a manner that, is truly scalable, reconfigurable, easily understood and thus optimized. The die design also offers independent control of the hole shape and configuration within a preform for the first time.

It is indeed an efficient and economic way to fabricate glass rods, tubes and MOF preforms with repeatable and controllable dimensions. A major benefit of the extrusion technique is that by avoiding the stacking procedure fewer interfaces are

involved and consequently lower losses than using other techniques can in principle be achieved.

1.4.3.2 Casting Technique

Casting of MOF preforms has been demonstrated with both glasses and polymers. This approach offers similar advantages as drilling compared to the stacking method, since the hole pattern, size and spacing can be altered independently in different structures while it does not create any unwanted interstitial holes within the lattice.

For glasses, MOF preform casting involves the use of the well-known low-temperature sol-gel technology. The sol-gel casting technique was originally developed for the production of large jacket tubes for optical fiber preforms and has been modified for the fabrication of PCFs. A number of micro-structured fibers fabricated using the sol-gel casting method [18]-[19] are shown in Fig 1.19.

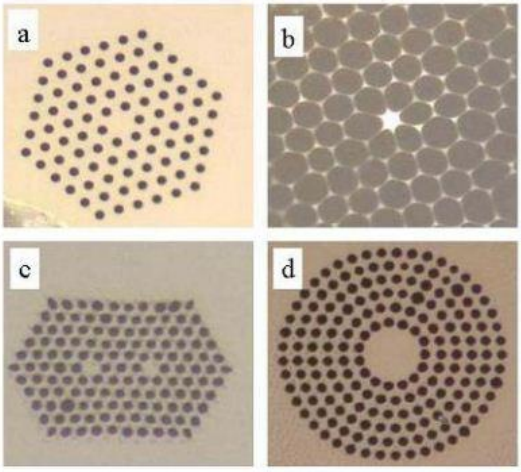

Fig 1. 19 Cross-sectional images of sol-gel derived micro-structured fibers. The dark regions correspond to air columns while the bright regions are silica. a) endlessly single-mode design, b) high delta, highly nonlinear fiber, c) dual core structure and d) circular core micro-structured fiber.

A mould containing an array of mandrel elements is assembled and then filled with colloidal silica dispersed at high pH with an average particle size of 40 nm. The pH is lowered causing the sol to gel. At the wet gel stage, the mandrel elements are removed, leaving air columns within the gel body. The gel body is then treated thermo-chemically to remove water and organic and transition metal contaminants. The dried porous gel body is then sintered near 1600° C into viscous glass and subsequently drawn into fiber. The mandrel elements are removed during the wet gel stage; while the gel body is still fragile. To fabricate fibers with high air-fill fractions the low air-fill fraction glass preforms have to be etched with hydrofluoric

acid uniformly along the length of the preform. The air holes are pressurized during draw to obtain the desired size and air-fill fraction. To maintain uniformity along the length of the preform, the mandrels are individually tensioned and the positioning and spacing is inspected and recorded with a digital camera. The aforementioned process is graphically represented in Fig 1.20.

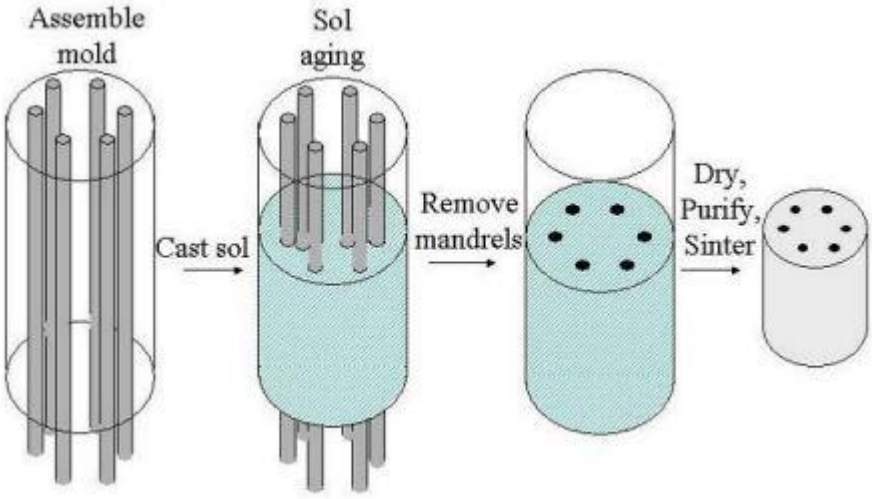

Fig 1. 20 Schematic representation of sol gel fabrication technique

As a casting method, the sol-gel technique can fabricate any structure, which can be assembled into a mold. The hole size, shape and spacing may all be adjusted independently. By comparison, stack and draw methods are limited to closest-packed geometries such as triangular or honeycomb lattices and cannot easily generate circular patterns such as the one shown in Fig 1.19 (d). Drilling methods allow adjustment of both the hole size and spacing, but are generally limited to a small number of holes and restricted to circular shapes. Furthermore, drilling of preforms leads to roughened surfaces along the air hole so that extra steps of etching and polishing of the inner surfaces are desired. Extrusion techniques provide design freedom, but are typically limited to soft glasses for which the material loss values are exceedingly high. Several designs such as fibers for higher nonlinearity, dispersion flattened designs [20] require independent spacing, hole size or even noncircular holes. The sol-gel casting method provides additional design flexibility that will be necessary for such fibers.

Chapter 2

Theoretical Analysis of PCF

2.1 Full Vector Finite Element Method

A finite element based optical mode solver is the most popular method to rigorously analyze photonic crystal fibers. Both the real and imaginary part of the modal indices can be computed in a relatively small computational domain.The leakage loss, the dispersion properties, the vectorial character, as well as the degeneracy of modes of the fibers can be studied through the finite element results.Since the introduction of the photonic crystal fiber (PCF), various wave guiding structures that utilize the arrangement of either circular or non-circular holes have been realized. The large variety of possible hole shapes and arrangements demand the use of numerical methods that can handle arbitrary cross-sectional shapes to analyze different kinds of structures. Besides, the existence of interfaces with high index-contrast between the solid host material and air holes call for the use of the vectorial wave equation to accurately model the structure. Finite element method (FEM) is suitable for such analysis as it can handle complicated structure geometries and solve vectorial equations transparently.

2.1.1 Analysis of FEM

Using FEM, any waveguide structure can be analyzed in a relatively small computational domain for its complex-valued modal indices and field profiles. The structures being considered may include those with either solid material or air as the core; circular or noncircular micro-structured holes arranged around the core. Through the FEM results, we have studied the leakage loss, dispersion properties, vectorial character, as well as the degeneracy of modes and single-modeness of particular kinds of PCFs.

The optical mode analysis is made on a cross-section in the x-y plane of the fiber. The wave propagates in the z-direction and has the form

$$\vec{H}(x,y,z,t) = \vec{H}(x,y)e^{-j(\omega t-\beta z)} \qquad (2.1)$$

Where ω is the angular frequency and β is the propagation constant. An Eigen value equation for the magnetic field, $\vec{H}$ is derived from Helmholtz equation

$$\nabla \times \left(n^{-2}\nabla \times \vec{H}\right) - {k_0}^2\vec{H} = 0 \qquad (2.2)$$

This can be solved for the eigenvalue of $\lambda = -j\beta$

The equation (2.2) is defined for longitudinally-invariant structures composed of non-magnetic anisotropic materials with diagonal permittivity tensors and $e^{j\omega t}$ time dependence

of the field; it is possible to get a vectorial wave equation expressed only in terms of the transverse components of the magnetic field as follows:

$$\begin{bmatrix} \partial_y \left[\frac{1}{{n_{zz}}^2}\left(\partial_x H_y - \partial_y H_x\right)\right] \\ -\partial_x \left[\frac{1}{{n_{zz}}^2}\left(\partial_x H_y - \partial_y H_x\right)\right] \end{bmatrix} - \begin{bmatrix} \frac{1}{{n_{yy}}^2}\partial_x\left(\partial_x H_x + \partial_y H_y\right) \\ \frac{1}{{n_{xx}}^2}\partial_y\left(\partial_x H_x + \partial_y H_y\right) \end{bmatrix} + {k_0}^2 {n_{eff}}^2 \begin{bmatrix} \frac{1}{{n_{yy}}^2} H_x \\ \frac{1}{{n_{xx}}^2} H_y \end{bmatrix} = {k_0}^2 \begin{bmatrix} H_x \\ H_y \end{bmatrix}$$

Here, the x and y denote the transverse Cartesian coordinates associated with the structure cross-section, k_0 the vacuum wavenumber, n_{eff} the complex modal index, H_x and H_y the x and y components of the magnetic field $\vec{H}$, ${n_{xx}}^2$, ${n_{yy}}^2$ and ${n_{zz}}^2$ the non-zero entries located at thediagonal of the relative permittivity tensor, associated with the x, y, and z components of the electric field, respectively. Discretizing the computational domain into triangular elements lead to the following discretized weak formulation:

$$\sum_{\substack{Boundary\ Element \\ e}} \left\{ -\int_{\Gamma_e} \frac{1}{{n_{zz}}^2} w_y\left(\partial_x H_y - \partial_y H_x\right) dy - \int_{\Gamma_e} \frac{1}{{n_{zz}}^2} w_x\left(\partial_x H_y - \partial_y H_x\right) dx \right.$$
$$\left. - \int_{\Gamma_e} \frac{1}{{n_{yy}}^2} w_x\left(\partial_x H_x + \partial_y H_y\right) dy + \frac{1}{{n_{xx}}^2} w_y\left(\partial_x H_x + \partial_y H_y\right) dx \right\} +$$

$$\sum_{\substack{Interface\ Element \\ e}} \left\{ -\int_{\Gamma_{int,e}} \frac{1}{{n_{yy}}^2} w_x\left(\partial_x H_x + \partial_y H_y\right) dy + \int_{\Gamma_{int,e}} \frac{1}{{n_{xx}}^2} w_y\left(\partial_x H_x + \partial_y H_y\right) dx \right\} +$$

$$\sum_{Triangular\ \ Element} \iint_{\Omega_e} \left\{ \frac{1}{{n_{zz}}^2}\left(\partial_x w_y - \partial_y w_x\right)\left(\partial_x H_y - \partial_y H_x\right) \right.$$
$$+ \left[\partial_x\left(\frac{1}{{n_{yy}}^2} w_x\right) + \partial_y\left(\frac{1}{{n_{xx}}^2} w_y\right)\right]\left(\partial_x H_x + \partial_y H_y\right)$$
$$\left. + k_0^2 n_{eff}^2 \left(\frac{1}{n_{yy}^2} w_x H_x + \frac{1}{n_{xx}^2} w_y H_y\right) - k_0^2\left(w_x H_x + w_y H_y\right) \right\} dxdy = 0$$

With w_x and w_y denoting the weight functions, Ω_e the area in each triangular element, $\Gamma_{int,e}$ the line element at the interface between different materials, and Γ_e the line element at the computational boundaries. Approximating the fields using quadratic nodal-based basis

functions will lead to a sparse generalized matrix eigenvalue equation, which can be solved using an eigenvalue solver to obtain the eigen values related to the modal indices (n_{eff}) and eigenvectors associated with the transverse components of the magnetic field $[H_x \quad H_y]^T$ of the corresponding nodes.

2.1.2 Boundary Conditions

During the numerical analysis, we have considered three types of boundary conditions. They are:

Perfect Electric Conductor:

This boundary condition can be expressed as,

$$n.B = 0$$

$$n \times E = 0$$

Here, n is the unit normal vector to the boundary. According to this condition, tangential components of E and normal components of B is continuous across any interface.

Perfect Magnetic Conductor:

This boundary condition can be expressed as,

$$n.D = 0$$

$$n \times H = 0$$

According to this condition, tangential components of H and normal components of D is continuous across any interface.

Perfectly Matched Layer

Numerical simulation of propagating waves in unbounded spatial domainsis a challenge common to many branches of engineering and applied mathematics. Perfectly matched layers (PML) are a novel technique for simulating the absorption of waves in open domains. The equations modeling the dynamics of phenomena of interest are usually posed as differential equations or integral equations which must be solved at every time instant. In many application areas like general relativity and acoustics, the underlying equations are systems of second order hyperbolic partial differential equations. In numerical treatment of such problems, the equations are often rewritten as first order systems and are solved in this form. For this reason, many existing PML models have been developed.

A perfectly matched layer is an artificial boundary condition implying perfect absorption of incident field. This boundary condition is required for approximating infinite zone beyond the waveguide outer edge to a finite domain of numerical analysis. Effect of PML on numerical solutions obtained will be more prominent when confinement of field in the PCF is weak. This layer can also be utilized to find out the complex part of effective index.

There are several different PML formulations. However, all PML's essentially act as a lossy material. The lossy material of lossy layer, is used to absorb the fields travelling away from the interior of the grid. The PML is anisotropic and constructed in such a way that there is no loss in the direction tangential to the interface between the lossless region and the PML. However, in the PML there is always loss in the direction normal to the interface.

The PML region can be viewed as a perfect absorber with a certain magnitude of conductivity. However, the optimized conductivity is calculated from certain sets of equations. In our work, we have considered cylindrical PML available in the commercial software [23].

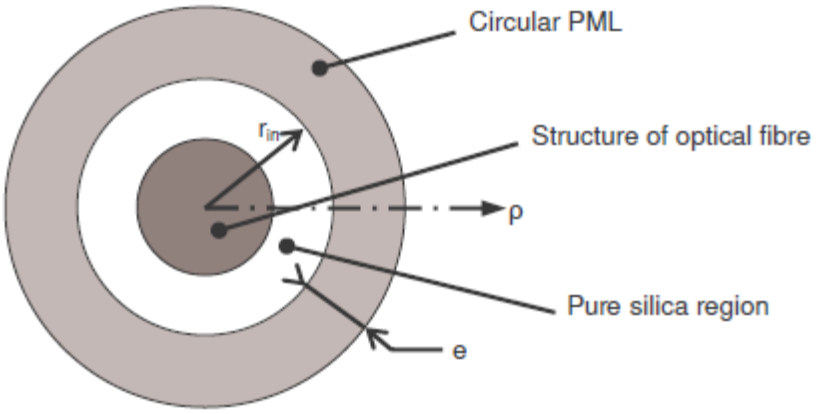

Fig 2. 1 PML region surrounding the waveguide structure.

Formulation of wave equations in the PML region can be done after rigorous analysis,

$$\Delta \times \bar{H} = j\omega n^2 s\bar{E}$$

$$\Delta \times \bar{E} = -j\omega\mu_0 s\bar{H}$$

$$s = 1 - j\frac{\sigma_e}{\omega n^2 \varepsilon_0} = 1 - j\frac{\sigma_m}{\omega\mu_0}$$

Where,
$\bar{E}$: Electric field
$\bar{H}$: Magnetic Field

σ_e: Electric conductivity of PML
σ_m: Magnetic conductivity of PML

e is the thickness of the PML layer which is ideally a multiple of the operating wavelength. To avoid numerical reflection, conductivity in the PML region is graded to a peak value rather than an abrupt rise as shown in fig 2.2

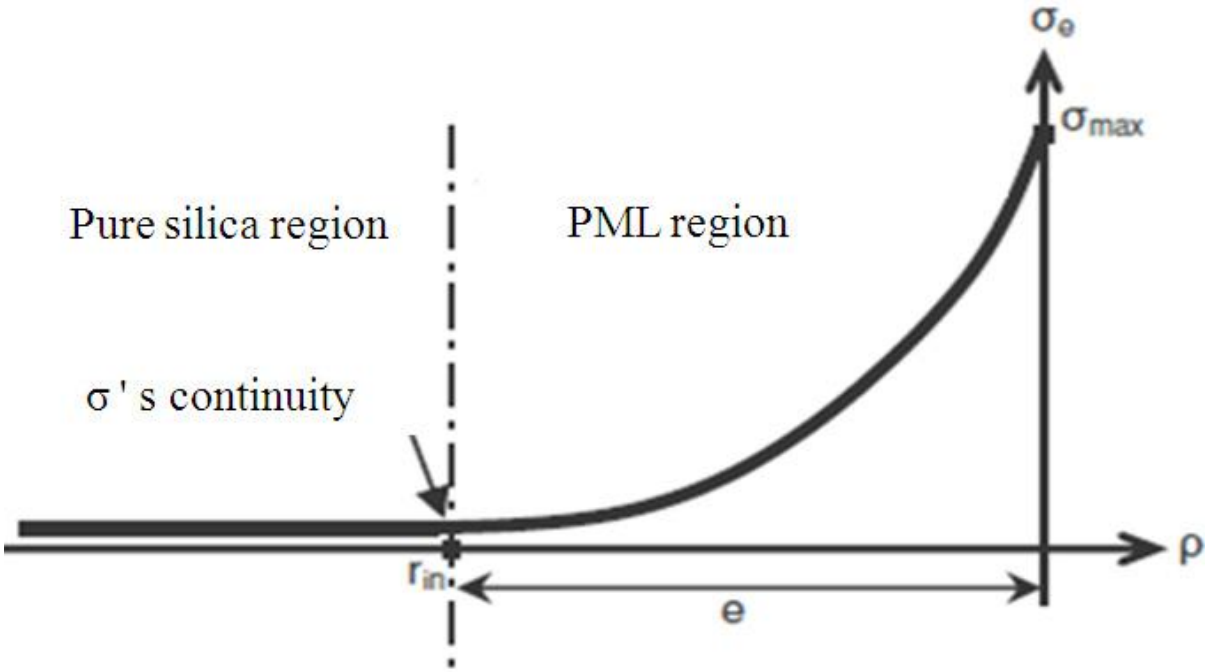

Fig 2. 2 Grading of PML conductivity

PML Parameters becomes,

$$s = \begin{cases} 1 - j.k\left(\dfrac{\rho - r_{in}}{e}\right)^2, & in\ PML\ region \\ 1 & in\ others\ region \end{cases}$$

Where, k is defined for wavelength λ by

$$k = \frac{3\lambda}{4\pi n_e}.\ln\left(\frac{1}{R}\right)$$

where R is the reflection coefficient of electromagnetic field from the interface to be minimized. For a perfectly matched condition to secure zero reflection from the interface, wecan write,

$$\frac{\sigma_e}{n^2\varepsilon_0} = \frac{\sigma_m}{\mu_0}$$

Now the reflection coefficient is defined as below [22]

$$R = \exp\left[\left(-2\frac{\sigma_{max}}{n\varepsilon_0 n_0}\int_0^d \left(\frac{\rho}{d}\right)^m\right)d\rho\right]$$

For this maximum conductivity is defined as below,

$$\sigma_{max} = \frac{m+1}{2}\frac{\varepsilon_0 cn}{d} ln\left(\frac{1}{R}\right)$$

Here, *m* is the order of polynomial for grading conductivity. These equations imply that, aminimum reflection will occur for a maximum conductivity. However, numerical error terms imply that there is an optimum magnitude of reflection for accurate propagation constant. A stable value of complex effective index can be obtained by altering the thickness of PML and distance of PML from center of the PCF.

2.1.3 Effective Index

Effective index is the key parameter for obtaining propagation characteristics of a PCF using modal analysis. The wave propagates in the z direction and has the form,

$$\vec{H}(x,y,z,t) = \vec{H}(x,y)e^{-j(\omega t - \beta z)}$$

where ω is the angular frequency and β is the propagation constant. An eigenvalue equation for the magnetic field, H for isotropic index is derived from Helmholtz equation.

$$\nabla \times \left(n^{-2}\nabla \times \vec{H}\right) - {k_0}^2\vec{H} = 0$$

This can be solved for the eigen-value of $\lambda = -j\beta$. When studying the characteristics of optical waveguides, the effective mode index of a confined mode,

$$n_{eff} = \frac{\beta}{k_0}$$

For confined mode in the core of the PCF,

$$n_2 < n_{eff} < n_1$$

where n_1 is the core index and n_2 is the clad index. The dispersion parameter D of the PCFs can be obtained from the wavelength dependence of the real part of the mode indices as follows,

$$D = -\frac{\lambda}{c}\frac{\partial^2}{\partial\lambda^2}Re(n_{eff})$$

while the attenuation due to leakage loss can be deduced from the imaginary part,

$$\alpha = -\frac{Loss}{L} = -20k_0 Im\left(n_{eff}\right)\log(e)$$

Chapter 3

Dispersion and Nonlinearity in a Silica Fiber

Intermodal dispersion in multimode fibers leads to considerable broadening of short optical pulses (~10ns/km). In the geometrical-optics description, such broadening was attributed to different paths followed by different rays. In the modal description it is related to the different mode indices (or group velocities) associated with different modes. The main advantage of single-mode fibers is that intermodal dispersion is absent simply because the energy of the injected pulse is transported by a single mode. However, pulse broadening does not disappear altogether. The group velocity associated with the fundamental mode is frequency dependent because of chromatic dispersion. As a result, different spectral components of the pulse travel at slightly different group velocities, a phenomenon referred to as group-velocity dispersion (GVD), intra-modal dispersion, or simply fiber dispersion. Intra-modal dispersion has two contributions, material dispersion and waveguide dispersion. We consider both of them and discuss how GVD limits the performance of light-wave systems employing single-mode fibers.

3.1 Group-Velocity Dispersion

Consider a single-mode fiber of length L. A specific spectral component at the frequency ω would arrive at the output end of the fiber after a time delay $T = \frac{L}{v_g}$, where v_g is the group velocity, defined as [24]

$$v_g = \left(\frac{d\beta}{d\omega}\right)^{-1}, \qquad (3.1)$$

The frequency dependence of the group velocity leads to pulse broadening simply because different spectral components of the pulse disperse during propagation and do not arrive simultaneously at the fiber output. If $\Delta\omega$ is the spectral width of the pulse, the extent of pulse broadening for a fiber of length L is governed by

$$\Delta T = \frac{dT}{d\omega}\Delta\omega = \frac{d}{d\omega}\left(\frac{L}{v_g}\right)\Delta\omega = L\frac{d^2\beta}{d\omega^2}\Delta\omega = L\beta_2\Delta\omega \qquad (3.2)$$

The dispersion parameter D can vary considerably when the operating wavelength is shifted from 1.3μm. The wavelength dependence of D is governed by the frequency dependence of the mode index. From Eq. (2.3.5), D can be written as

$$D = -\frac{2\pi c}{\lambda^2}\frac{d}{d\omega}\left(\frac{L}{v_g}\right) = -\frac{2\pi}{\lambda^2}\left(2\frac{d\bar{n}}{d\omega} + \omega\frac{d^2\bar{n}}{d\omega^2}\right) \qquad (3.3)$$

D can be written as the sum of two terms,

$$D(\lambda) = D_w(\lambda) + D_m(\lambda) \qquad (3.4)$$

3.2 Material Dispersion

Material dispersion occurs because the refractive index of silica, the material used for fiber fabrication, changes with the optical frequency component. On a fundamental level, the origin of material dispersion is related to the characteristic resonance frequencies at which the material absorbs the electromagnetic radiation. Far from the medium resonances, the refractive index $n(\lambda)$ is well approximated by the Sellmeier equation [25]

$$n^2(\lambda) = 1 + \frac{B_1\lambda^2}{\lambda^2 - C_1} + \frac{B_2\lambda^2}{\lambda^2 - C_2} + \frac{B_3\lambda^2}{\lambda^2 - C_3} \qquad (3.5)$$

For silica glass the parameters are found to be B_1=0.80686642, B_2=0.71815848, B_3= 0.85416831, C_1= 0.068972606μm, C_2= 0.15396605μm, C_3 = 11.841931μm.

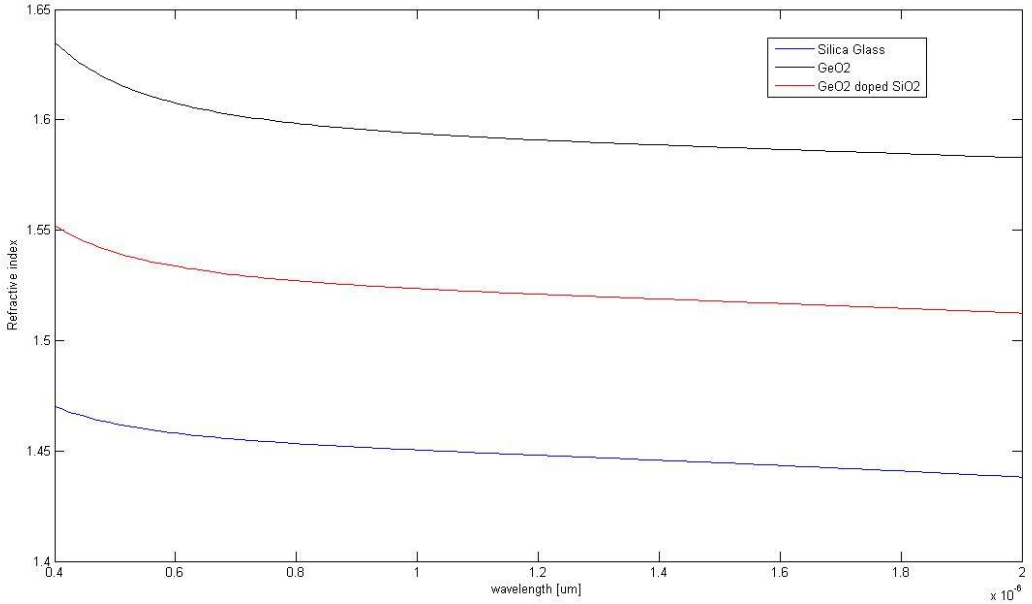

Fig 3. 1 Wavelength dependence of n in the range 0.4-2μm for silica, GeO_2 and GeO_2 doped SiO_2

3.3 Waveguide Dispersion

The contribution of waveguide dispersion $D_w(\lambda)$ to the dispersion parameter D is given by

$$D_W = -\frac{2\pi\Delta}{\lambda^2}\left[\frac{n_{2g}^2 d}{n_2\omega}\frac{Vd^2(Vb)}{dV^2} + \frac{dn_{2g}}{d\omega}\frac{d(Vb)}{dV}\right] \qquad (3.6)$$

and depends on the V parameter of the fiber. It turns out that $D_w(\lambda)$ is negative in the entire wavelength range 0-1.6μm. On the other hand, $D_m(\lambda)$ is negative for wavelengths below λ_{ZD} and becomes positive above that. Figure 3.2 shows $D_m(\lambda)$,

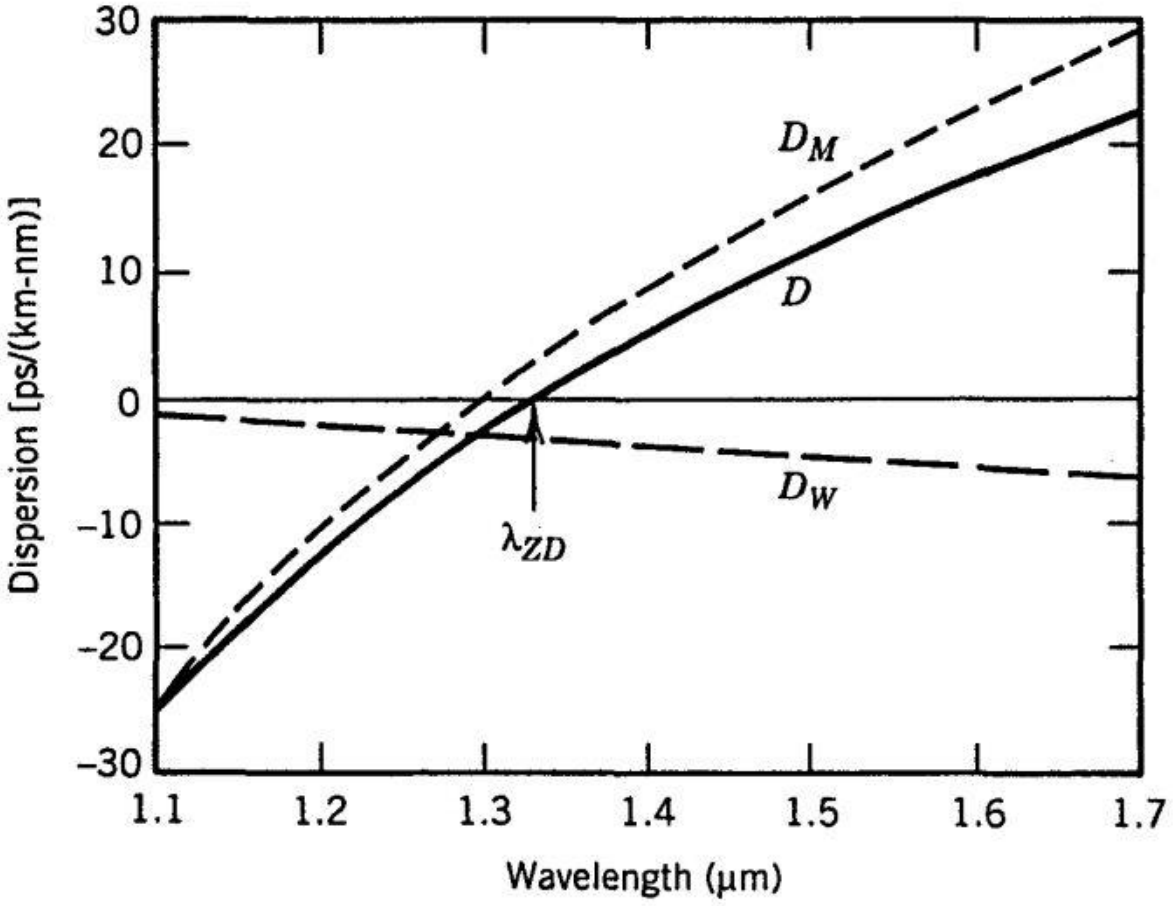

Fig 3. 2 Total dispersion D and relative contributions of material dispersion Dm(λ) and waveguide dispersion Dw(λ) for a conventional single-mode fiber. The zero-dispersion wavelength shifts to a higher value because of the waveguide contribution.

$D_w(\lambda)$ and their sum $D(\lambda)=D_w(\lambda)+D_m(\lambda)$, for a typical single-mode fiber. The main effect of waveguide dispersion is to shift λ_{ZD} by an amount 30-40 nm so that the total dispersion is zero near 1.31μm. It also reduces D from its material value $D_m(\lambda)$ in the wavelength range 1.3-1.6μm that is of interest for optical communication systems. Typical values of D are in the range of 15 to 18 ps/(km-nm) near 1.55μm. This wavelength region is of considerable interest for lightwave systems because fiber losses become minimum near 1.55μm. High values of D limit the performance of 1.55μm lightwave systems.

Since the waveguide contribution $D_w(\lambda)$ depends on fiber parameters such as the core radius a and the index difference A, it is possible to design the fiber such that λ_{ZD} is shifted into the vicinity of 1.55μm [26]-[27]. Such fibers are called dispersion shifted fibers. It is also possible to tailor the waveguide contribution such that the total dispersion D is relatively small over a wide wavelength range extending from 1.3 to 1.6μm [28]-[30]. Such fibers are called dispersion-flattened fibers. The design of dispersion modified fibers involves the use of multiple cladding layers and a tailoring of the refractive-index profile [26]-[32]. Waveguide dispersion can also be used to produce dispersion-decreasing fibers in which GVD decreases along the fiber length because of axial variations in the core radius. In another kind of fibers, known as the dispersion-compensating fibers, GVD is made normal and has a relatively large magnitude. Table 3.1 lists the dispersion characteristics of several commercially available fibers.

Fiber Type and Trade Name	A_{eff} (μm^2)	λ_{ZD} (μm^2)	D(C Band) [ps/(km-nm)]	Slope S [ps/(km-nm^2)]
Corning SMF-28	80	1302-1322	16-19	0.090
OFS AllWave	80	1300-1322	17-20	0.088
Draks ColorLock	80	1300-1320	16-19	0.090
Corning Vascade	100	1300-1310	18-20	0.060
OFS TrueWave-RS	50	1470-1490	2.6-6	0.050
Corning LEAF	72	1490-1500	2.0-6	0.060
Draka TeraLight	65	1430-1440	5.5-10	0.052

Table 3. 1 Characteristics of several commercial fibers [33]

3.4 Dispersion Management

Optical amplifiers solve the fiber-loss problem but, at the same time, make the dispersion problem worse because dispersive effects keep accumulating along the entire chain of amplifiers. Indeed, long-haul WDM systems making use of amplifiers are often limited by the dispersive and nonlinear effects rather than fiber losses. However, the dispersion problem can be managed in practice through a suitable dispersion-compensation scheme. This chapter focuses on several such techniques. Section 3.4.1 explains the basic idea behind dispersion management. Section 3.4.2 is devoted to special kinds of fibers developed for compensating dispersion in long-haul links. Several types of dispersion-equalizing filters are discussed in this section.

3.4.1 Dispersion Problem and Its Solution

All long-haul lightwave systems employ single-mode optical fibers in combination with distributed feedback (DFB) semiconductor lasers with a relatively narrow line width (<0.1 GHz). The performance of such systems is often limited by pulse broadening induced by group-velocity dispersion (GVD) of silica fibers. Direct modulation of a DFB laser chirps optical pulses in an optical bit stream and broadens their spectrum enough that direct modulation cannot be used at bit rates above 2.5 Gb/s. WDM systems operating at channel bit rates of 10Gb/s or more often employ external modulators to avoid spectral broadening induced by frequency chirping. Under such conditions, the GVD-limited transmission distance at a given bit rate B is obtained

$$L < \frac{1}{16|\beta_2|B^2} = \frac{c\pi}{8\lambda^2|D|B^2} \qquad (3.7)$$

where β_2 is related to the commonly used dispersion parameter D. For "standard" telecommunication fibers D is about 16ps/(km-nm) near λ=1.55um. Equation (3.7) predicts that L cannot exceed 30 km at a bit rate of 10Gb/s when such fibers are used for designing lightwave systems.

One may think that the dispersion problem can be solved for new fiber links by employing dispersion-shifted fibers and operating the link close to the zero-dispersion wavelength of this fiber so that D≈ 0. Under such conditions, system performance is limited by third-order dispersion (TOD).

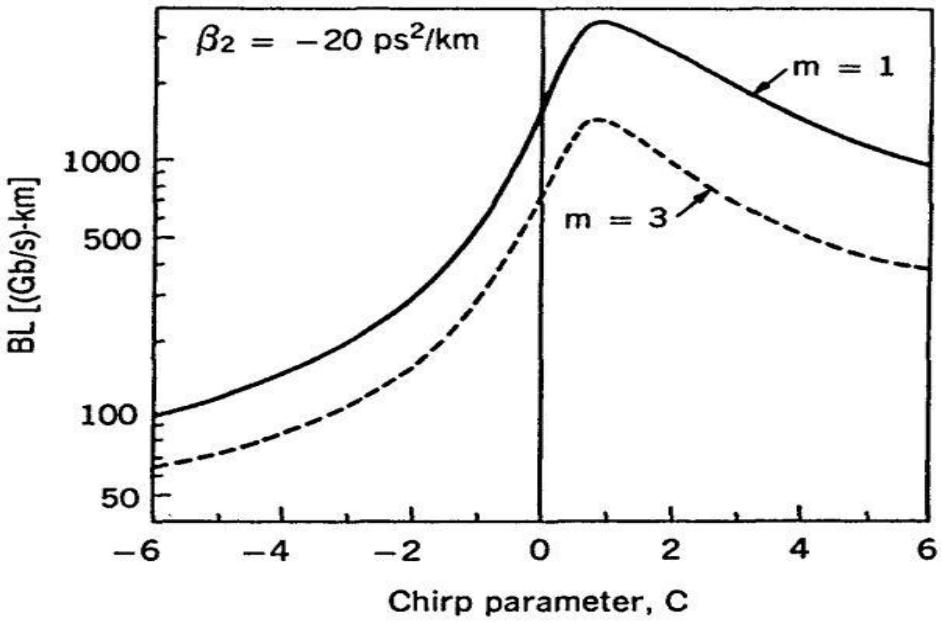

Fig 3. 3 Dispersion-limited BL product as a function of the chirp parameter for Gaussian (solid curve) and super-Gaussian (dashed curve) input pulses.

The dashed line in Fig 3.3 shows the maximum possible transmission distance at a given bit rate B when D = 0. Indeed, such a system can operate over more than 1,000 km even at a bit

rate of 40 Gb/s. However, this solution is not practical for WDM systems because of four-wave mixing (FWM). The nonlinear phenomenon of FWM becomes quite efficient for low values of the dispersion parameter D and limits performance of any system operating close to the zero-dispersion wavelength of the fiber. For this reason, some form of dispersion management is employed for all long-haul WDM systems [35]-[37].

The basic idea behind any dispersion-management scheme is quite simple

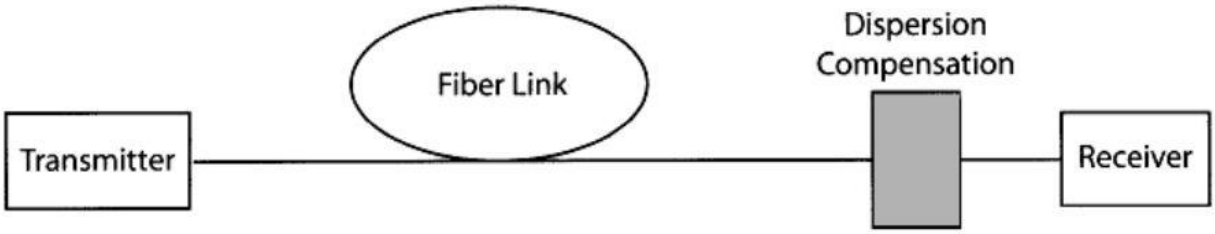

Fig 3. 4 Schematic of a dispersion-compensation scheme in which an optical filter is placed before the receiver.

3.4.2 Dispersion-Compensating Fibers

Optical filters whose transfer function has the form $H(\omega) = H_f * L(\omega)$ are not easy to design. The simplest solution is to use an especially designed fiber as an optical filter because it automatically has the desired form of the transfer function. This solution was suggested as early as 1980 [38] and it provides an all-optical, fiber-based solution to the dispersion problem. During the 1990s, a special kind of fiber, known as the dispersion-compensating fiber (DCF), was developed for this purpose [39]-[45]. Such fibers are routinely used for upgrading old fiber links or for installing new WDM fiber links. Such a scheme works well even when the nonlinear effects are not negligible as long as the average optical power launched into the fiber link is optimized properly.

In terms of the dispersion parameter D and the dispersion slope S the conditions for perfect dispersion compensation are:

$$L_1D_1+L_2D_2=0 \qquad S_1D_1+S_2D_2=0 \qquad (3.8)$$

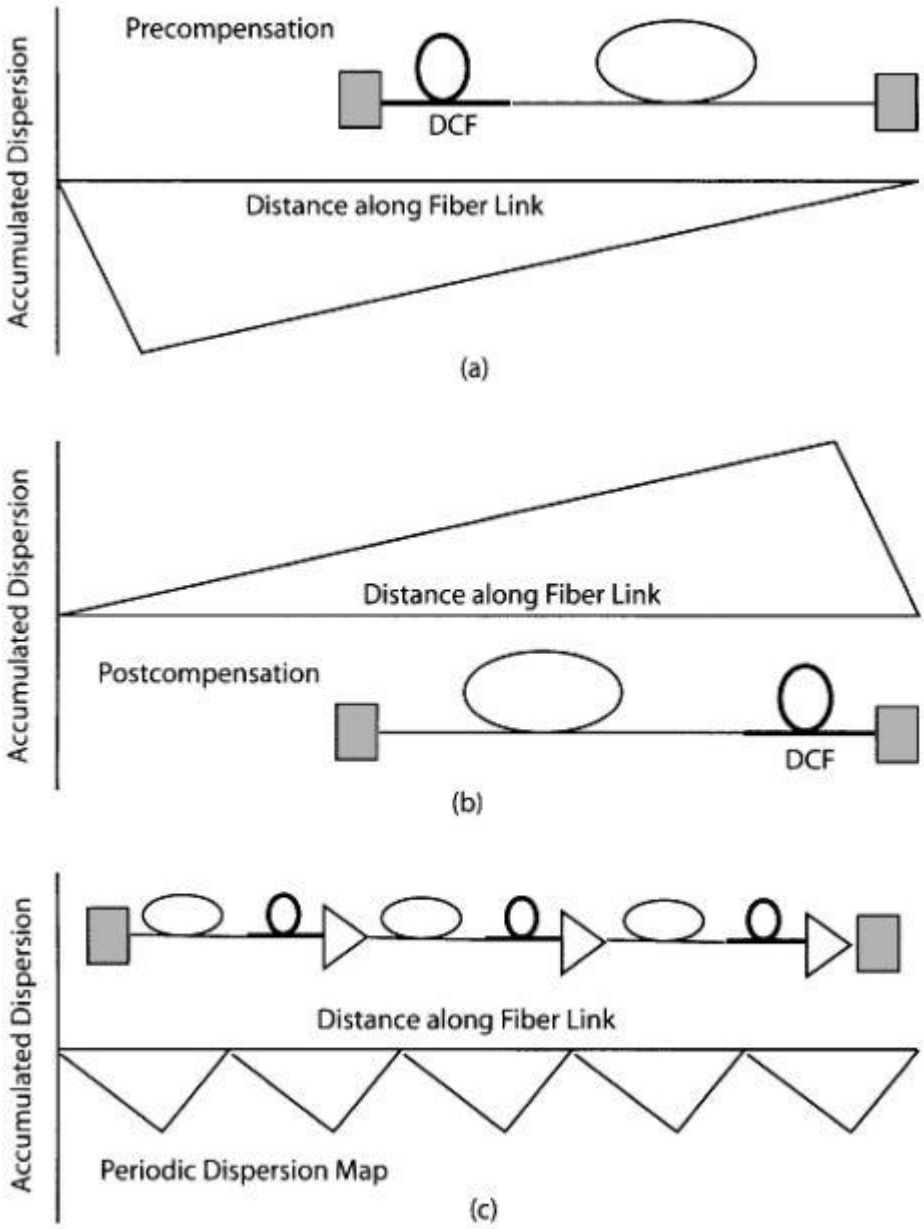

Fig 3. 5 Schematic of three dispersion-management schemes: (a) pre-compensation, (b) post-compensation, and (c) periodic compensation. In each case, accumulated dispersion is shown along the link length.

3.5 Fiber Non-Linearity

Three major nonlinear effects occurring inside optical fiber are self-phase modulation (SPM), cross-phase modulation (XPM), four-wave mixing (FWM) are governed by a single nonlinear parameter γ. For most optical fibers γ has a value of $\sim 1W^{-1}$/km. It was realized during the 1990s that this value is too small for optical fibers to be useful as a nonlinear medium for practical applications. To solve this problem, several new kinds of fibers with γ>10 W−1/km have been developed, and they are collectively referred to as highly nonlinear fibers.

3.5.1 Nonlinear Parameter

The nonlinear parameter γ can be written as

$$\gamma = \frac{2\pi n_2}{\lambda A_{eff}} = \frac{2\pi \iint_s n_2(x,y) I_s{}^2(x,y)\, dxdy}{\lambda\left(\iint_s I_s(x,y)\, dxdy\right)}$$

where λ is the wavelength of light and A_{eff} is the effective mode area given in

$$A_{eff} = \frac{(\iint_s |E_t|^2\, dxdy)^2}{\iint_s |E_t|^4\, dxdy}$$

This area depends on the fiber design, and it can be reduced with a proper design to enhance γ. On the other hand, the nonlinear-index coefficient n_2 is a material parameter related to the third-order susceptibility. This parameter is fixed for each glass material. Thus, the only practical approach for enhancing γ for silica-based optical fibers is to reduce the effective mode area A_{eff}. The use of non-silica glasses provides an alternative approach to designing highly nonlinear fibers. Before focusing on the design of such fibers, it is important to discuss the techniques used to determine n_2 experimentally. Accurate measurements of both γ and A_{eff} are necessary for this purpose.

3.5.2 Units and Values of n_2

The growing importance of the nonlinear effects in optical fibers revived interest in the measurements of γ during the 1990s, especially because fiber manufacturers are often required to specify the numerical value of γ for their fibers [46]. Several different experimental techniques have been developed to measure n_2 and applied to different types of fibers [47]–[56]. They make use of one of the nonlinear effects discussed in earlier chapters. In fact, all of the three major nonlinear effects SPM, XPM and FWM have been used for this purpose. All techniques measure γ and deduce n_2 from it. Table 3.2 summarizes the results obtained in several experiments using standard, dispersion-shifted (DSF), or dispersion-compensating fibers (DCFs) in the wavelength region near 1550 nm. Measured values are found to vary in the range of 2.2 to 3.9×10−20 m^2/W. The uncertainty in n_2 values depends not only on the measurement errors associated with γ but also on how accurately one can estimate the effective mode area A_{eff} from the mode-field diameter. In the remainder of this section, we discuss various measurement techniques and indicate why they may yield different values of n_2 even at the same wavelength.

Method used	λ (μm)	Fiber type	Measured n_2 ($10^{-20}m^2/W$)	Experimental conditions
SPM	1.319	Silica core	2.36	110-ps pulses [36]
	1.319	DSF	2.62	110-ps pulses [36]
	1.548	DSF	2.31	34-ps pulses [37]
	1.550	DSF	2.50	5-ps pulses [40]
	1.550	Standard	2.20	50-GHz modulation [41]
	1.550	DSF	2.32	50-GHz modulation [41]
	1.550	DCF	2.57	50-GHz modulation [41]
XPM	1.550	Silica core	2.48	7.4-MHz modulation [38]
	1.550	Standard	2.63	7.4-MHz modulation [38]
	1.550	DSF	2.98	7.4-MHz modulation [38]
	1.550	DCF	3.95	7.4-MHz modulation [38]
	1.548	Standard	2.73	10-MHz modulation [42]
	1.548	Standard	2.23	2.3-GHz modulation [42]
FWM	1.555	DSF	2.25	Two CW lasers [35]
	1.553	DSF	2.35	10-ns pulses [39]

Table 3. 2 Measured values of n_2 for different fibers [57]

Chapter 4

Results and Discussions

4.1 Dispersion properties of PCF with different number of air hole layer at cladding region.

Different types of cladding and core structure of PCFs, consisting of an array of micrometer sized air-holes that allows flexible tailoring of the dispersion curve. Control of dispersion in PCFs is very important problem for realistic application of optical fiber communication. Several designs for the PCFs have been proposed to achieve the ultra-flattened dispersion properties. Conventional PCF designs the air holes arrayed in a rectangular lattice with all the same air-hole diameter. Fig 4.1-4.8 shows the different types of structure of varying number of air hole with solid core as well as same diameter of air hole in hexagonal lattice structure.

For all the designs we chose same material air-hole, solid core and PML. For core and PML we chose Silica Glass (SiO_2).

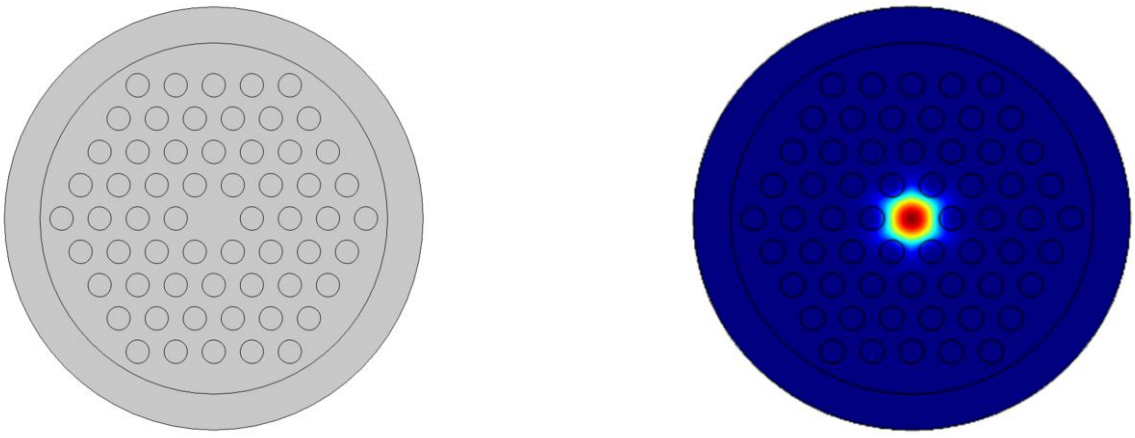

(a) (b)

Fig 4.1(a) Regular 4 layers Hexagonal PCF with solid core (b) fundamental mode of the structure.

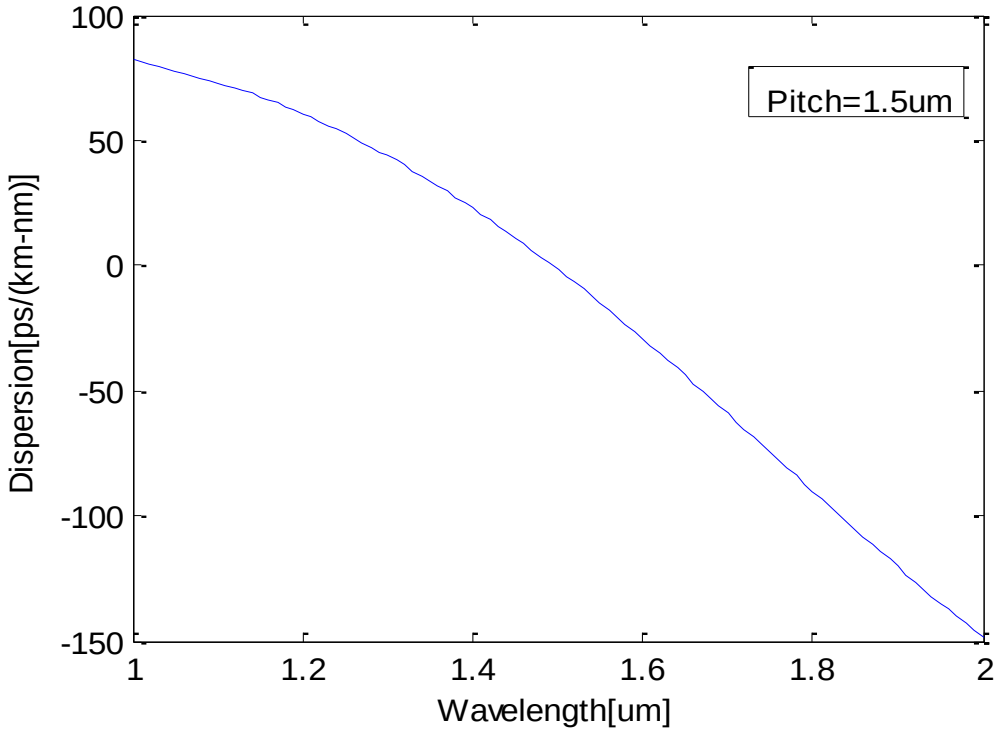

Fig 4.2 Dispersion of the selective 4 layers solid core Hexagonal PCF for lattice constant Λ=1.5μm and air hole diameter d=.53* Λ.

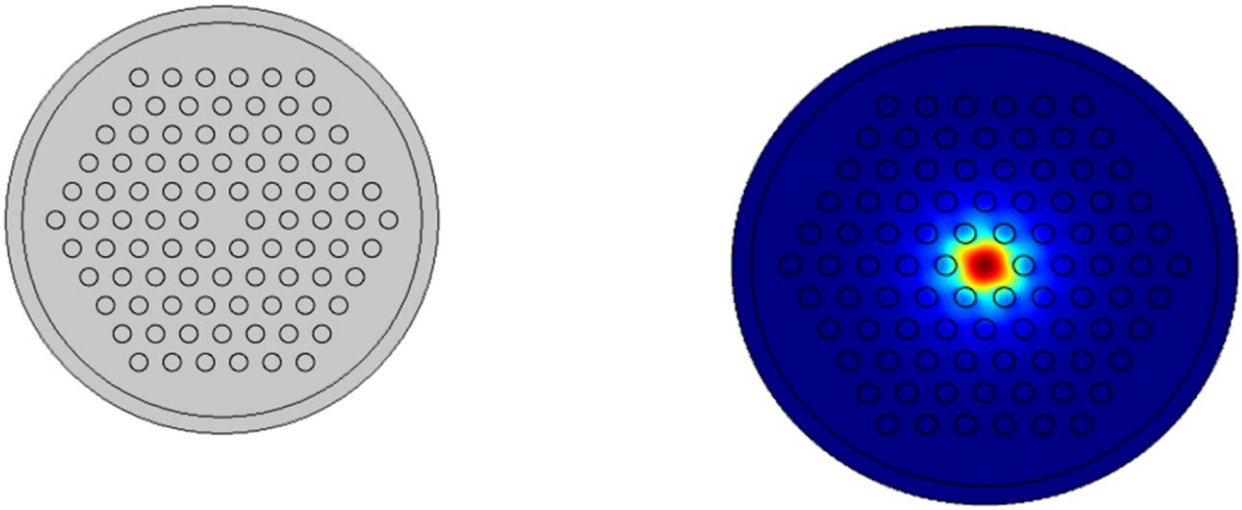

(a) (b)

Fig 4.3 (a) Five layers solid core Hexagonal PCF (b) fundamental mode of the structure

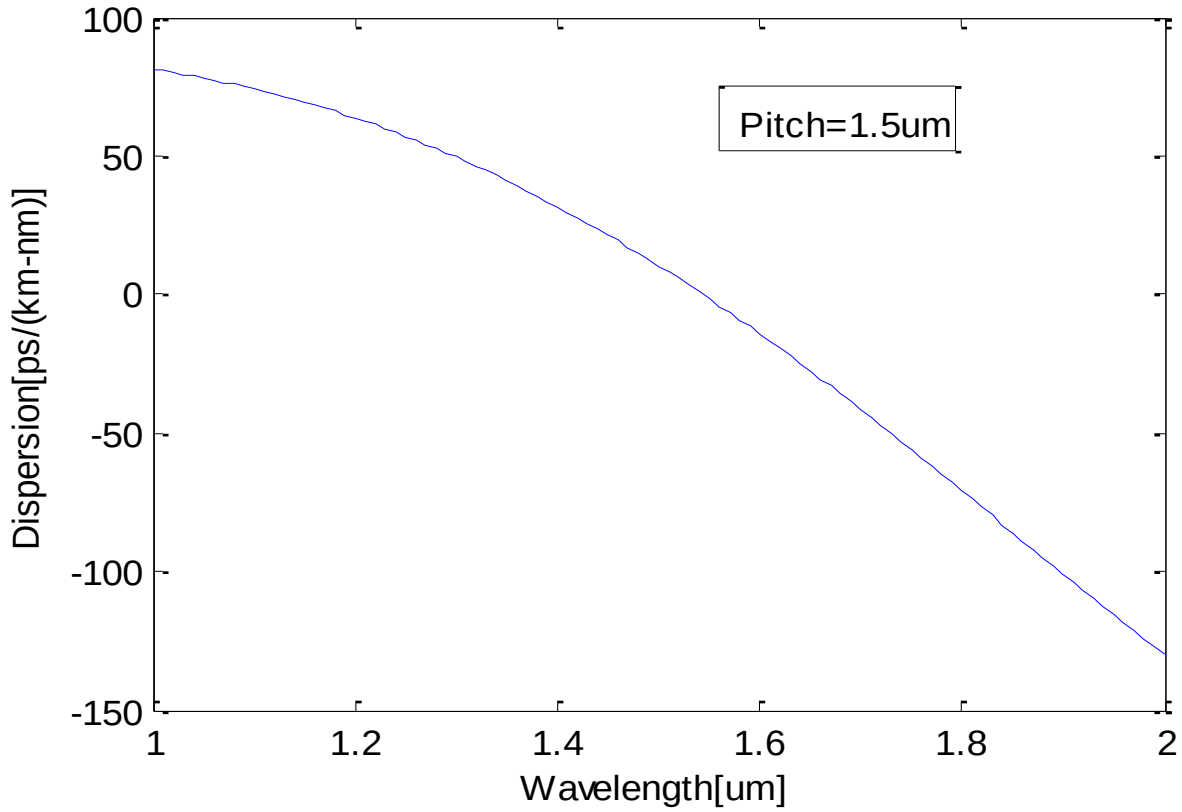

Fig 4.4 Dispersion of the selective 5 layers solid core Hexagonal PCF for lattice constant Λ=1.5μm and air hole diameter d=.53* Λ.

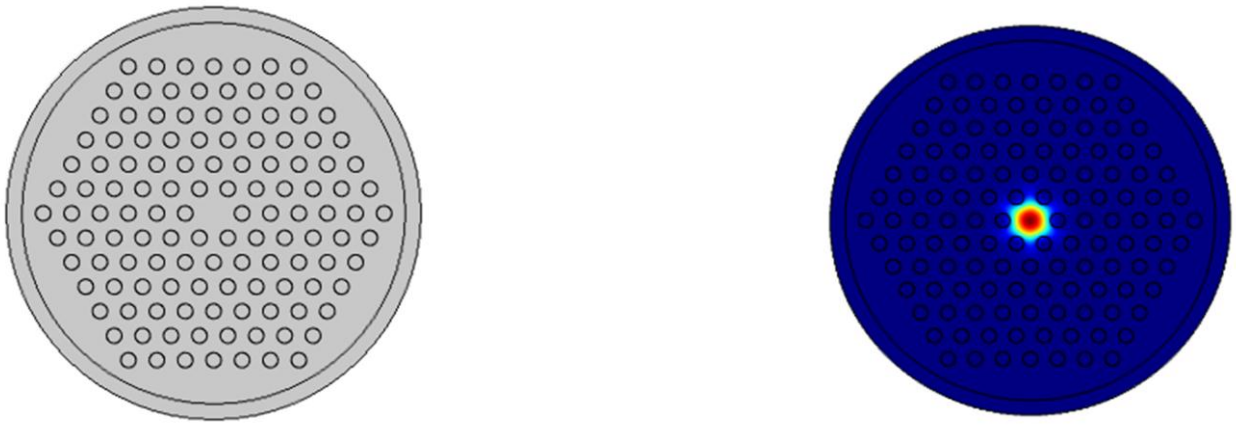

(a) (b)

Fig 4.5 (a) Six layer solid core Hexagonal PCF (b) Fundamental mode of the structure.

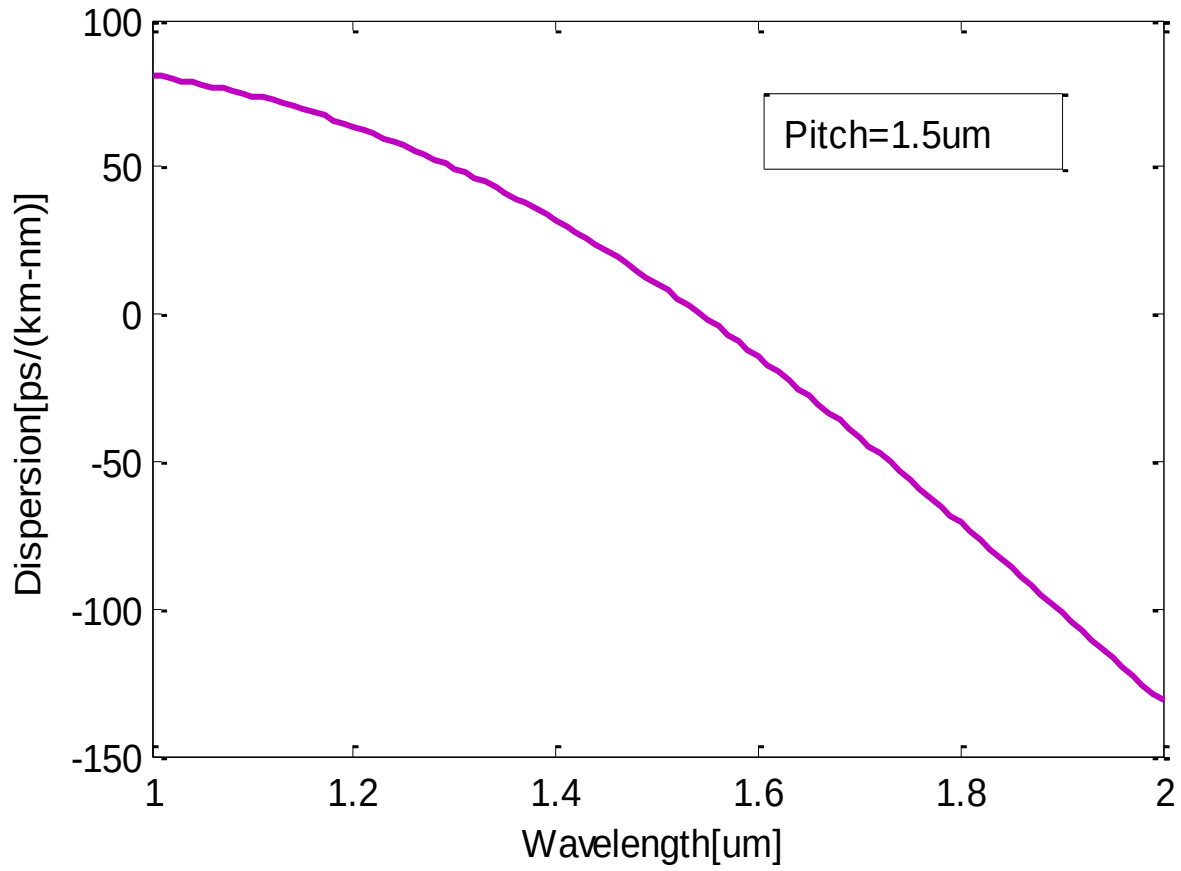

Fig 4.6 Dispersion of the selective 6 layers solid core Hexagonal PCF for lattice constant Λ=1.5μm and air hole diameter d=.53a.

We see the dispersion curve for 4, 5 and 6 layers. The design has been done at same lattice constant that is pitch Λ=1.5um and air-hole diameter d=.53a. The material has been chosen for those designs are also kept same. The cladding region consists air-hole and solid core made by silica (SiO_2).PML region also made by silica glass (SiO_2).

From the dispersion curves 4.2, 4.4 and 4.6 we see that in every case the dispersion goes to down steps with the increasing the wavelength. That is dispersion decreasing with the increasing of wavelength for any number of air hole layer we used. From the figure 4.7 we see that the regional dispersion achieved for 4 layer air-hole. That's why we chose for layer air hole in the cladding which is full of air for our further work to get Ultra-flattened Dispersion of any PCF.

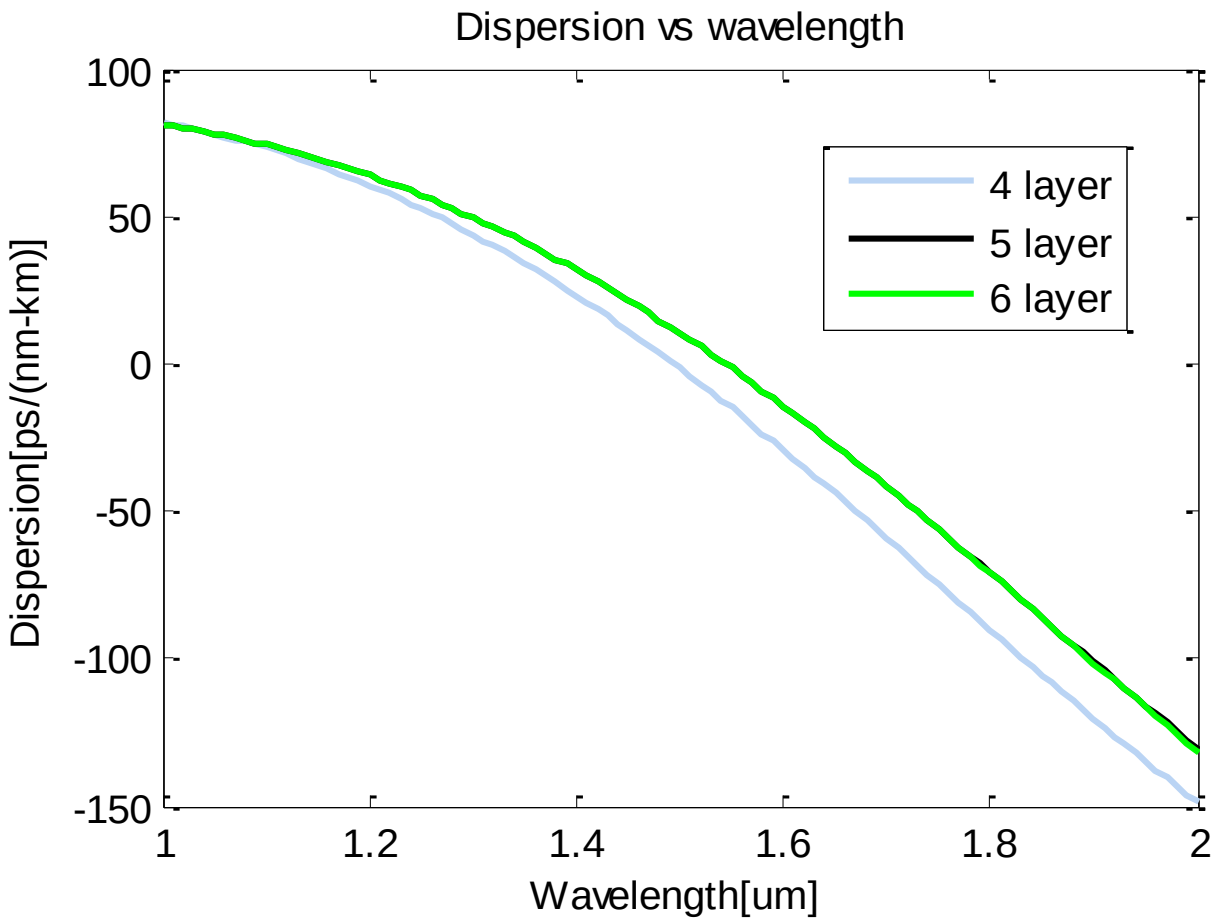

Fig 4.7 Shows the micro adjustment of the dispersion curves for 4(blue line), 5(black line) and 6(green line) layer at lattice constant Λ=1.5μm and air-hole diameter d=.53a.

For different number of layer of air hole at the same pitch we gate Effective Refractive Index at every wavelength. From the effective refractive index vs wavelength curve we see that the line does not cut the zero line. So we can say for every wavelength we get a value of effective refractive index. Fundamental mode was selected to see for which effective refractive index value the total light passes through the core region. That is total Electric Field passes through the core region.

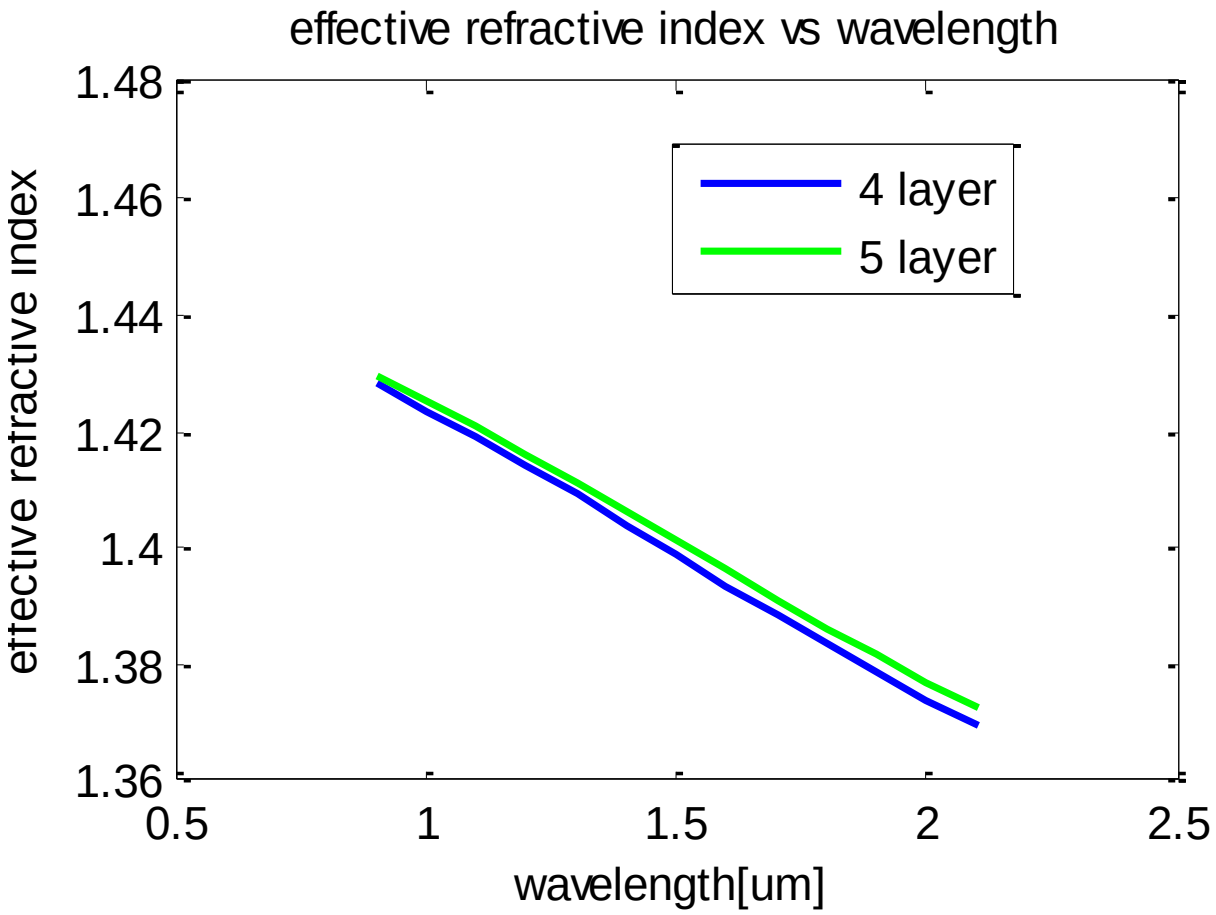

Fig 4.8 Effective Refractive Index vs Wavelength for 4 and 5 air-hole layers Hexagonal solid Core Λ=1.5μm and d=.53Λ.

4.2 Ultra-flattened Dispersion Controllability Using a Circular Defected-Core PCF

The PCF structure in the fig 4.9 present a novel systematic solution to the problem of controlling the chromatic dispersion and dispersion slope in photonic crystal fibers (PCFs), using a structurally-simple PCF with a defected-core. By adjusting the size of the central air- hole defect, ultra-flattened PCF as well as small effective mode area were achieved [58]. The design strategy is based on the mutual cancellation between the waveguide and the material dispersions of the PCF, by varying the size of the central defected region in the core. The verification of the ultra-flattened chromatic dispersion property of the proposed PCF is ensured with an accurate full-vector finite element method with anisotropic perfectly matched layers. The ultra-flattened dispersion feature and the small effective mode area are the main advantages of the PCF structure in fig 4.9 [58].

The hexagonal regular structure with the circular defected air hole in the core region is shown in the fig 4.9 with its fundamental mode.

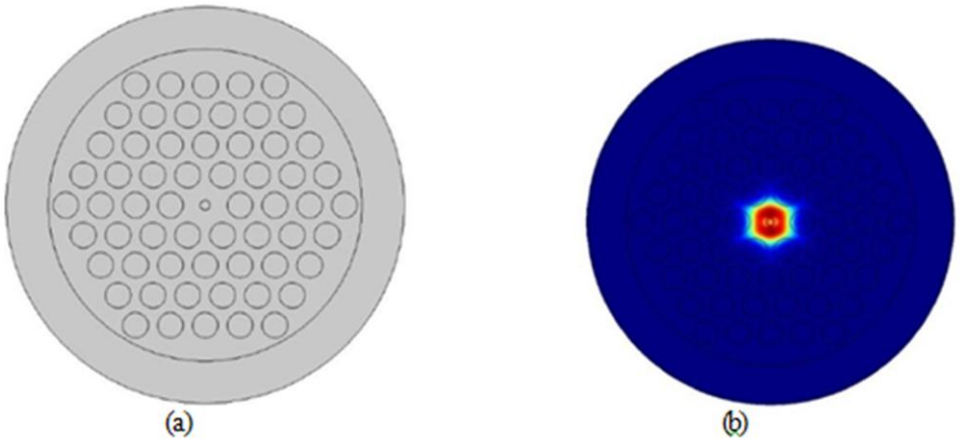

Fig 4. 9(a) Regular Hexagonal PCF structure with defected air hole (b) fundamental mode of the ultra-flattened hexagonal structure

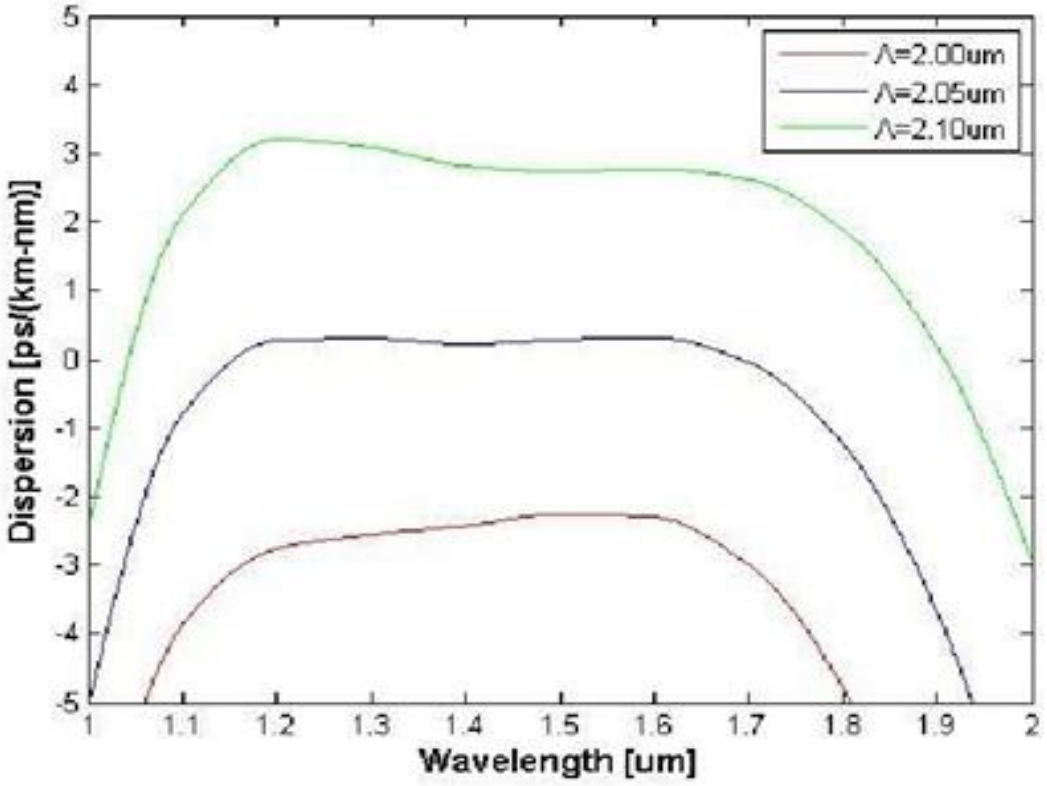

Fig 4. 10 Impact of the micro-adjustment of the design parameters in the total dispersion curve of the PCF for lattice constant Λ=2.0 μm (red line), Λ=2.05 μm (blue line), Λ=2.1 μm (green line)

In fig 4.10, 4.11 and 4.12 the optimized design parameters corresponding to the total dispersion indicated with blue lines, are Λ=2.05 μm, d/Λ=0.73, and dc/Λ=0.279.

Different structure of photonic crystal fiber shows different dispersion and non linear properties. To reduce dispersion and improve non linearity, crystal structure may be of hexagonal, octagonal or others shape. Design of a PCF is highly dependent on its application and choice of certain materials in different bands of wavelengths.

To reduce dispersion and improve non linear parameters in the certain range, We propose a regular hexagonal PCF structure with GeO_2 doped SiO_2 square defected Core

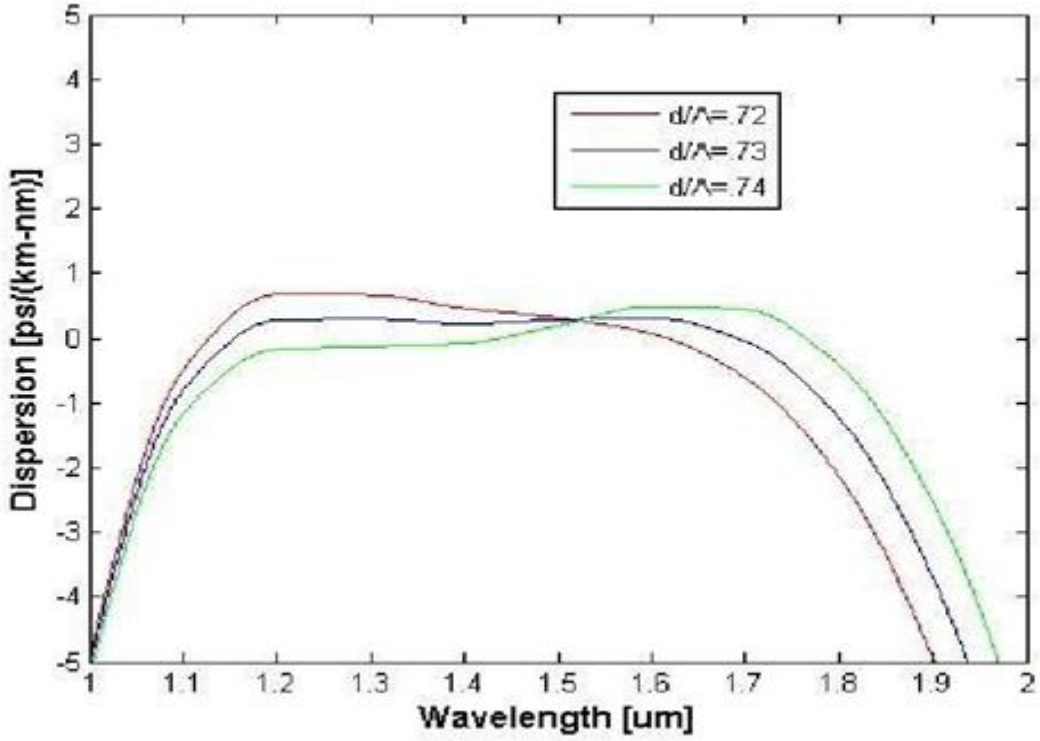

Fig 4. 11 Impact of the micro-adjustment of the design parameters in the total dispersion curve of the PCF for diameter of cladding air-holes, d/Λ=0.72 (red line), d/Λ=0.73 (blue line), d/Λ=0.74 (green line)

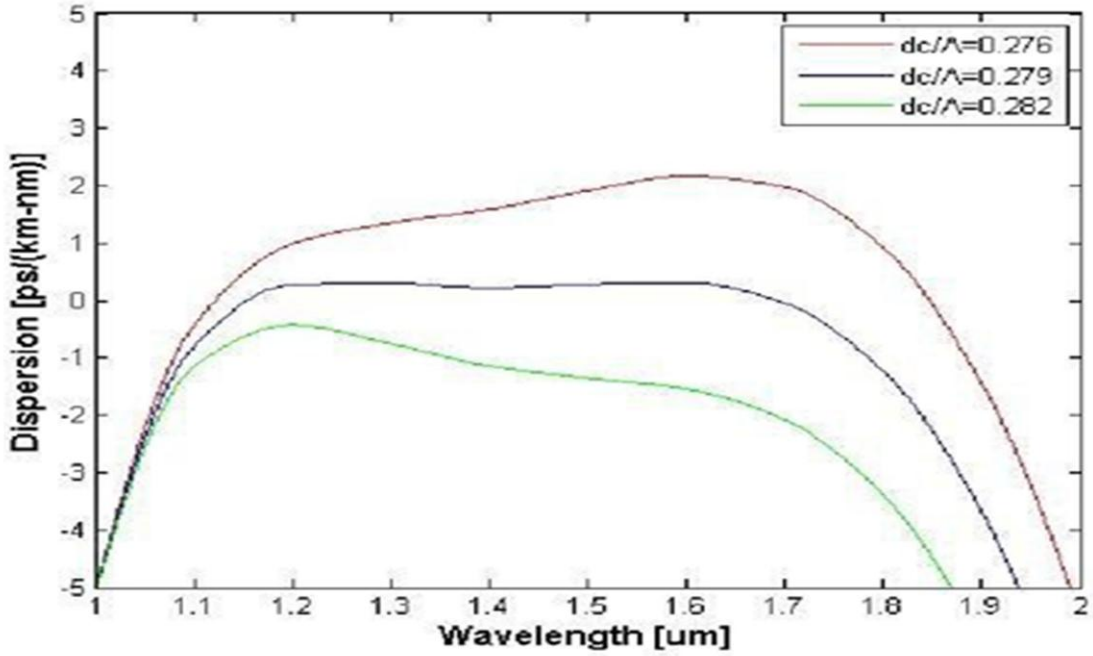

Fig 4. 12 Impact of the micro-adjustment of the design parameters in the total dispersion curve of the PCF for diameter of the defected air-holes, dc/Λ=0.276 (red line), dc/Λ=0.279 (blue line), dc/Λ=0.282 (green line)

4. 3 A Novel Design of Dispersion Flattened Fiber With High Nonlinear Parameter

Fig 4.5 shows the regular hexagonal photonic crystal fiber structure with triangular arrangement of air holes in the cladding region. Where „Λ" is the lattice constant, „d" is the air hole diameter and „a" is the side length of the square defected core and square defected core material is GeO_2 doped SiO_2.

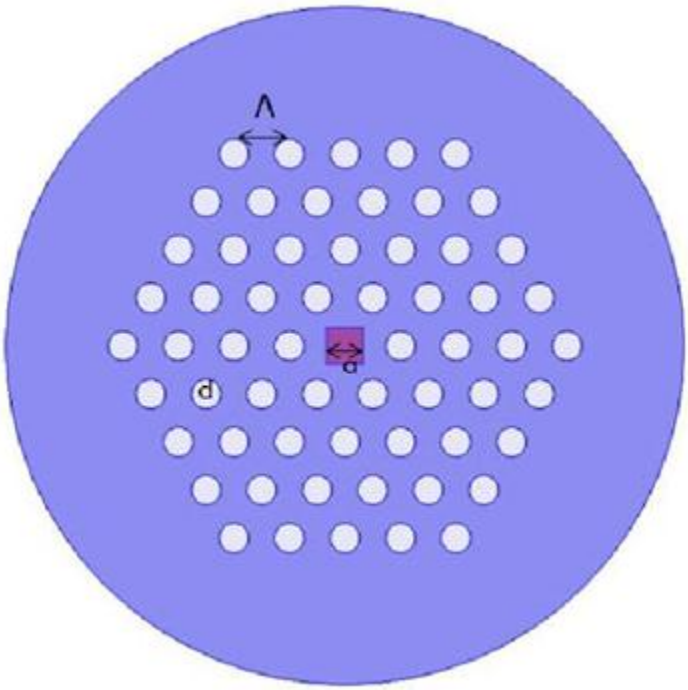

Fig 4. 13 Geometrical model of the proposed PCF with GeO2 doped SiO2 square defected core.

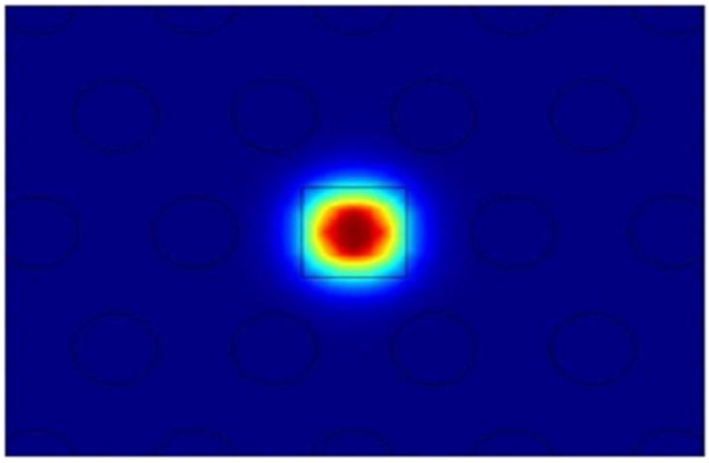

Fig 4. 14 Cross section of the magnetic field distribution of the fundamental mode of fig 4.13

4. 3.1 Numerical Result of Dispersion Properties

In this work the optimized structural parameters are Λ=1.55μm, a /Λ =1.325 and d/Λ=0.53.

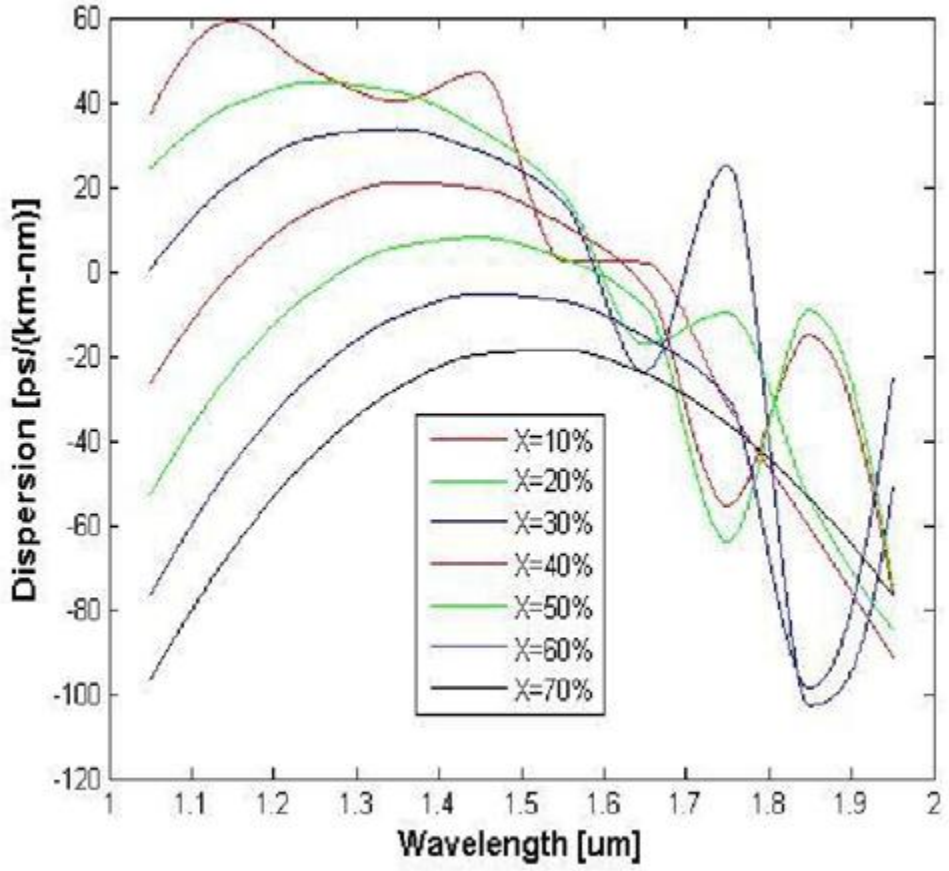

Fig 4. 15 Dispersion profile of the proposed structure as function of wavelength at different doping concentration

In fig 4.15 we show the total dispersion versus wavelength for different doping concentration of GeO_2 .it can be seen here dispersion is nearly zero between the doping concentrations of GeO_2 at 50% to 60%. And for increasing the doping concentration dispersion profile shifts downward. We further simulated for several doping concentration between 50% and 60% and we got optimum doping concentration at 53.23% at which total dispersion is 0.0002ps/ (km- nm).

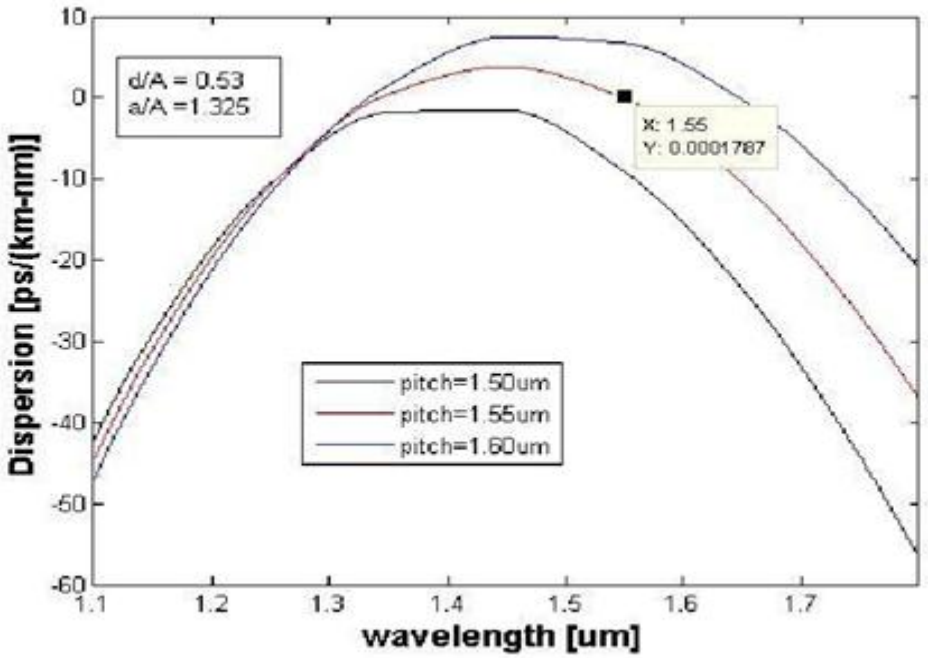

Fig 4. 16 Dispersion profile of the proposed structure as function of wavelength at 53.23 % doping concentration with the variation of pitch

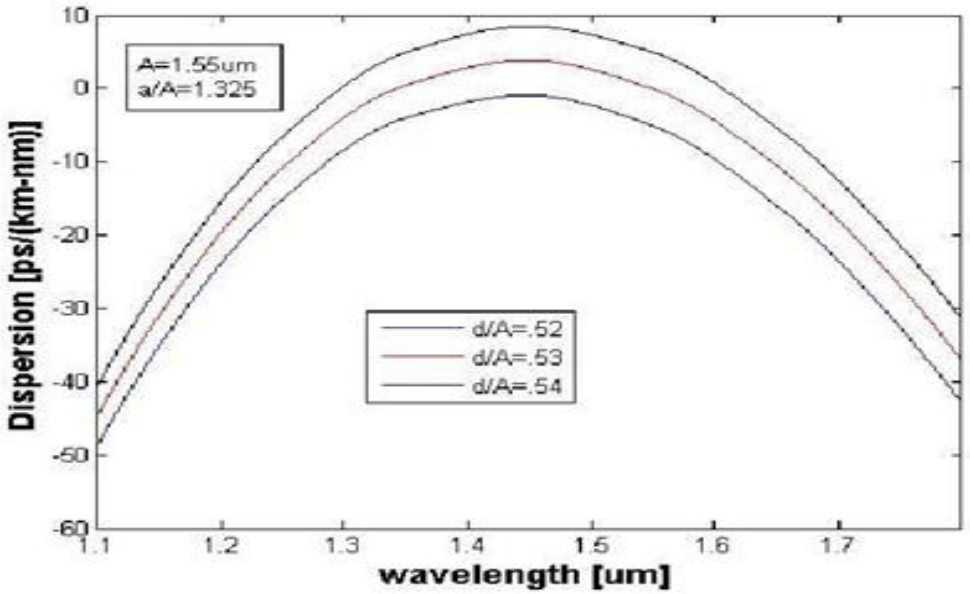

Fig 4. 17 Dispersion profile of the proposed structure as function of wavelength at 53.23 % doping concentration with the variation of air hole diameter

In fig 4.16 we show the total dispersion versus wavelength for different lattice constant. At d/ Λ=0.53 and a/ Λ=1.325, it can be seen here dispersion is nearly zero at operating wavelength 1.55μm. And for increasing the lattice constant dispersion profile shifts upward.

In fig 4.17 we show the total dispersion versus wavelength for different air hole diameter. At Λ=1.55μm and a/ Λ=1.325, it can be seen here dispersion is nearly zero at operating wavelength 1.55μm. And for increasing the air hole diameter dispersion profile shifts downward

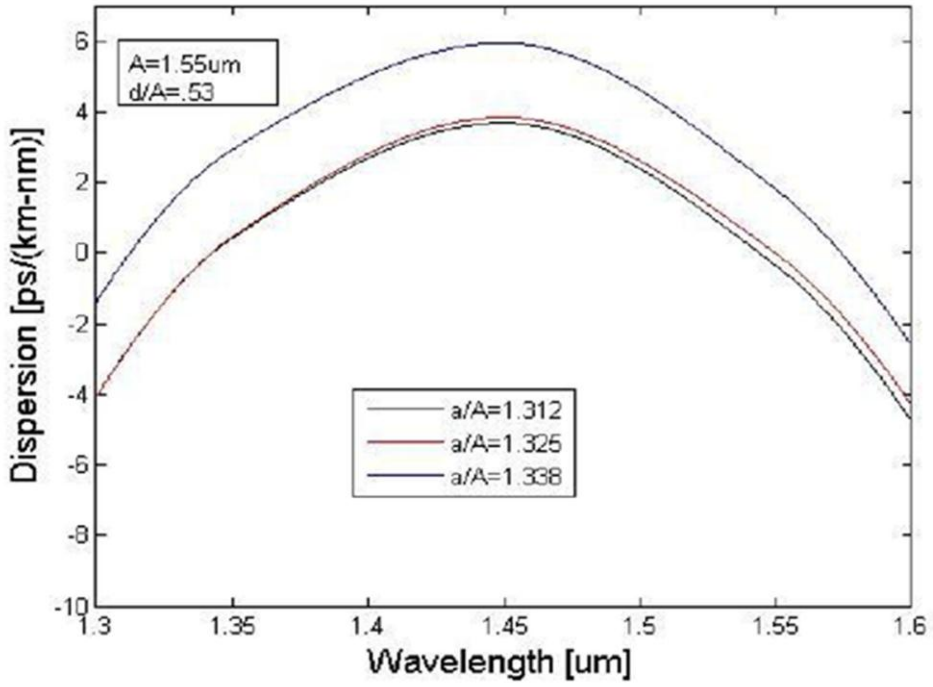

Fig 4. 18 Dispersion profile of the proposed structure as function of wavelength at 53.23 % doping concentration with the variation of side length of the square defected core

In fig 4.18 we found that the total dispersion versus wavelength for different side length of the square defected core. At Λ=1.55μm and d/ Λ=0.53, it can be seen here dispersion is nearly zero at operating wavelength 1.55μm. And for increasing the air hole diameter dispersion profile shifts upward.

4.3.2 Numerical Result of Nonlinear Properties

The empirical relation between the refractive index and the wavelength. The equation is used to determine the dispersion profile. The sellmeier equation for the silica glass is

$$n^2(\lambda) - 1 = \sum_{i=1}^{3} \frac{B_i \lambda^2}{\lambda^2 - C_i} \qquad (4.1)$$

Where, n is the refractive index, λ is the wavelength and B_1, B_2, B_3 and C_1, C_2, C_3 are determined sellmeier coefficients.

Similarly the sellmeier equation for GeO_2 doped SiO_2 is given by [59],

$$n^2(\lambda) - 1 = \sum_{i=1}^{3} \frac{[SA_i + X(GA_i - SA_i)]\lambda^2}{\lambda^2 - [Sl_i + X(Gl_i - Sl_i)]^2} \qquad (4.2)$$

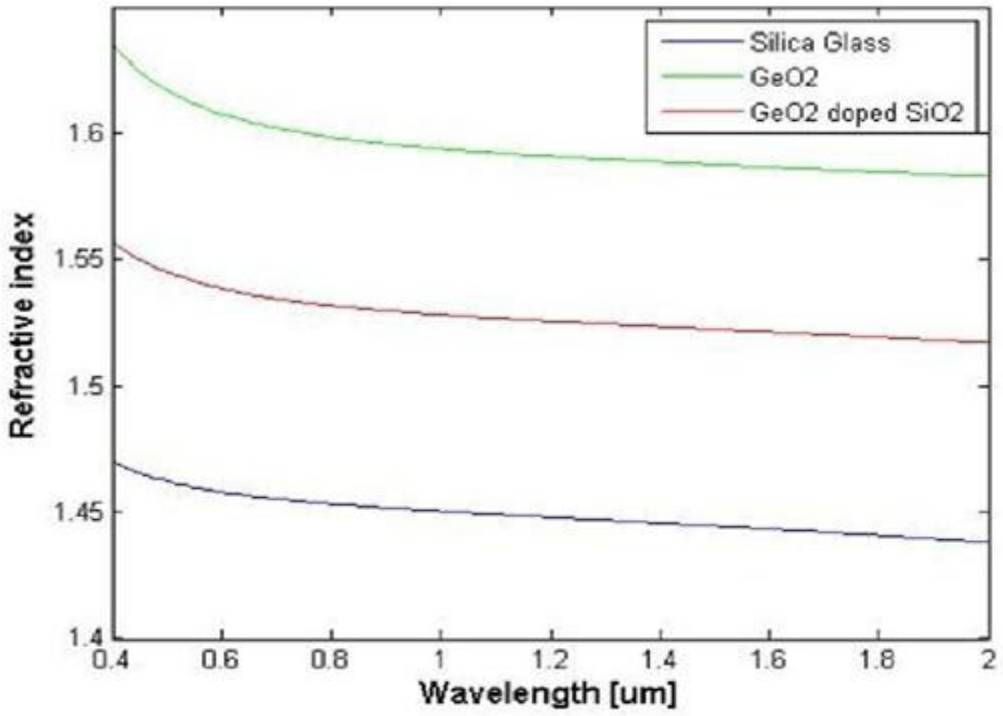

Fig 4. 19 Refractive index of silica glass (blue line), GeO2 (green line) and GeO2 doped SiO2(red line) as a function of wavelength

In fig 4.19, refractive index versus wavelength is plotted using the equation (4.1) and (4.2) for silica glass, $GeO2$, and GeO_2 doped SiO_2 .

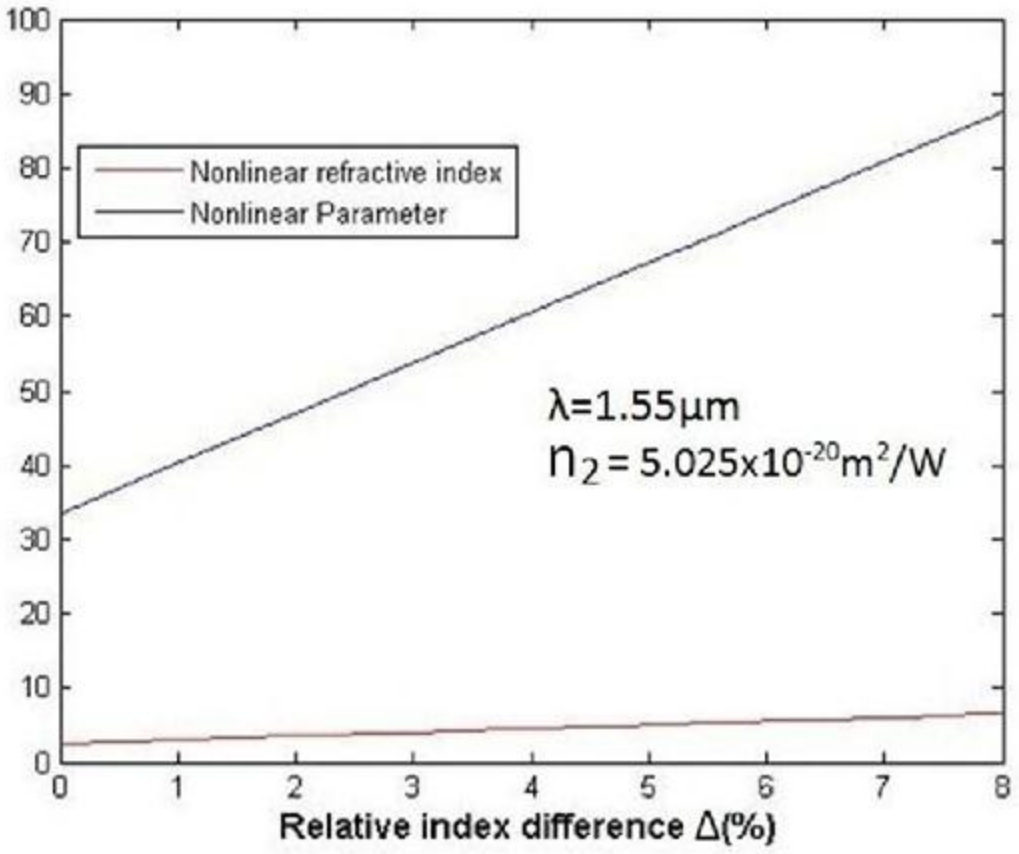

Fig 4. 20 Nonlinear refractive index and nonlinear parameter as function of relative index difference

$$\Delta = \frac{n_1^2 - n_0^2}{2n_1^2} \qquad (4.3)$$

$$n_2 = 2.507 + 0.505\Delta \qquad (4.4)$$

n_0=refractive index of pure silica
n_1=refractive index of fiber core doped with GeO_2
n_2=non-linear refractive index of pure silica

In fig 4.20, nonlinear refractive index and nonlinear parameter is plotted as function of relative index difference where we can see that as nonlinear parameter increases nonlinear refractive index also increases.

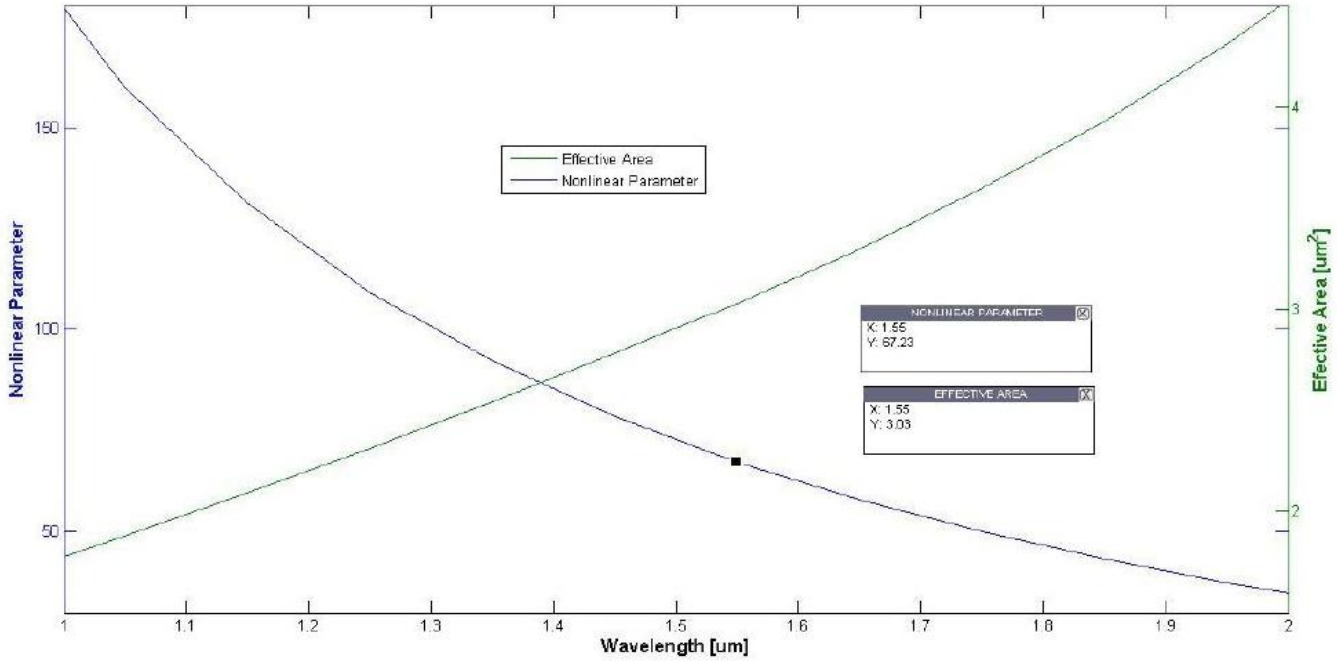

Fig 4. 21 Nonlinear Parameter and Effective Mode area as a function of wavelength

In fig 4.21, effective mode area increases with the wavelength. Since nonlinear parameter is inversely proportional to the effective mode area, consequently nonlinearity parameter decreases with the increasing wavelength. At operating wavelength 1.55μm the effective mode area and non linearity parameter is 3.03μm^2 and 67.23 $W^{-1}km^{-1}$ respectively.

4.4 Another Novel Design of Dispersion Flattened Fiber with Maximum Nonlinear Parameter at Lower Doping Concentration.

Fig 4.22 shows the regular hexagonal photonic crystal fiber structure with triangular arrangement of air hole in the cladding region also nearest air-hole diameter of the core is half of the other air hole. Where **"**Λ" is the lattice constant, "a" is the air-hole diameter, "dc" is the side length of the square defected core and "d1" is the diameter of the nearest surrounding air-hole of the core region. The square defected core material is **GeO_2 doped SiO_2**.

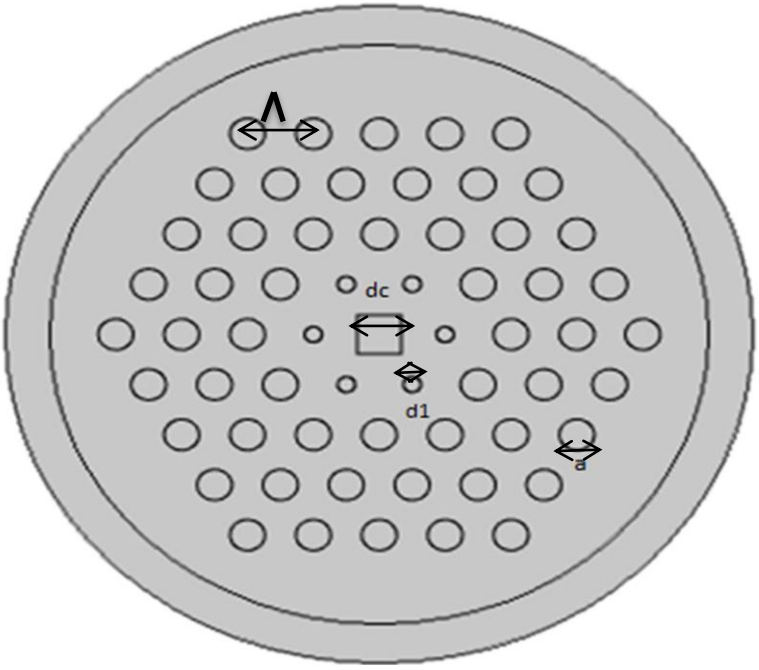

Fig 4.22 Geometrical mode of the proposed PCF with GeO2 doped SiO2 square defected core and nearest air-hole diameter half of the other air-hole diameter.

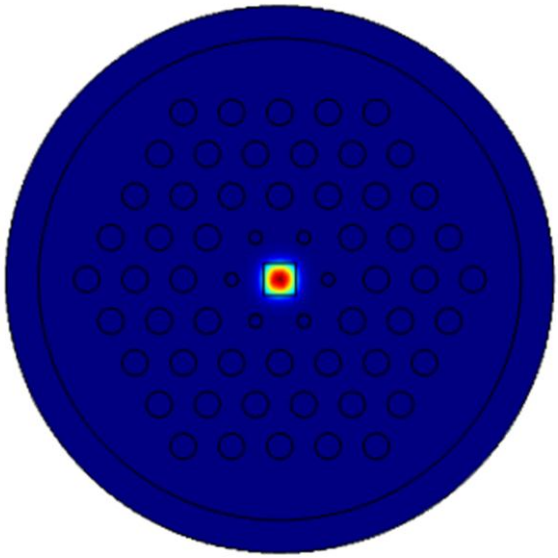

Fig 4.23 Cross section of the magnetic field distribution of the fundamental mode of fig 4.22.

4.4.1Numerical Result of Dispersion Properties

In this work the optimized structure parameter are Λ=3μm, dc/Λ=1.338, a/Λ=.53 and d1=d/2.

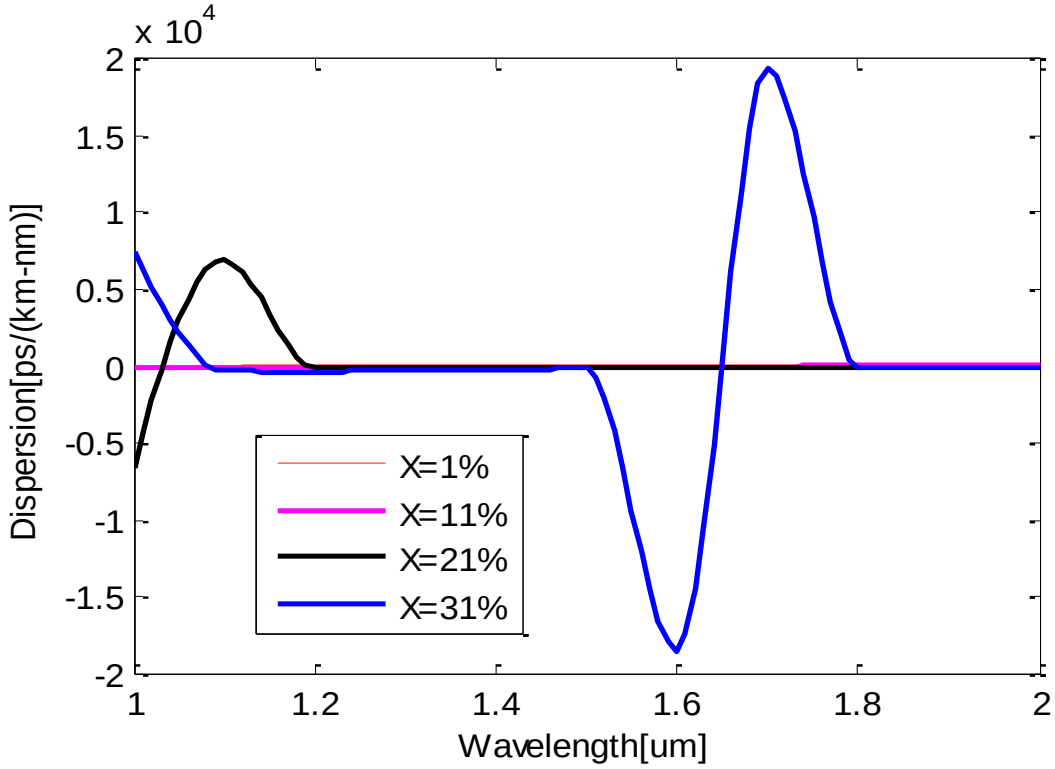

Fig 4.24 Dispersion profile of the proposed structure as a function of wavelength at different doping concentration.

In fig 4.24 we show the total dispersion versus wavelength for different doping concentration of **GeO_2**. It can be seen here dispersion is nearly zero could not be achieved perfectly for any doping concentration. If we see the dispersion curve from fig 4.25 for doping concentration 1% for the above design parameters we get a better flattened dispersion curve than other doping concentration. And increasing the doping concentration from 1% the dispersion profile shifts downward. We further simulated for several doping concentration between 1% and 11% and we got optimum doping concentration at 1% at which total dispersion is .5682ps/(km-nm).

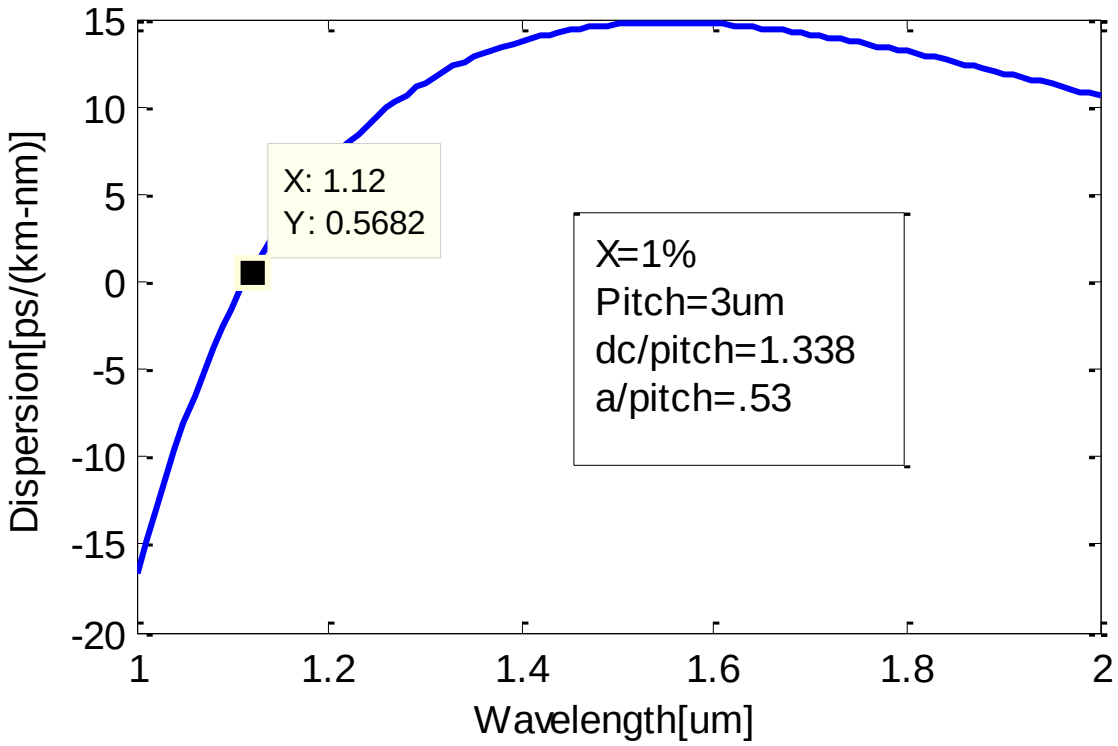

Fig 4.25 Dispersion profile of the proposed structure as function of wavelength at 1% doping concentration with pitch Λ=3μm, dc/Λ=1.338, a/Λ=.53.

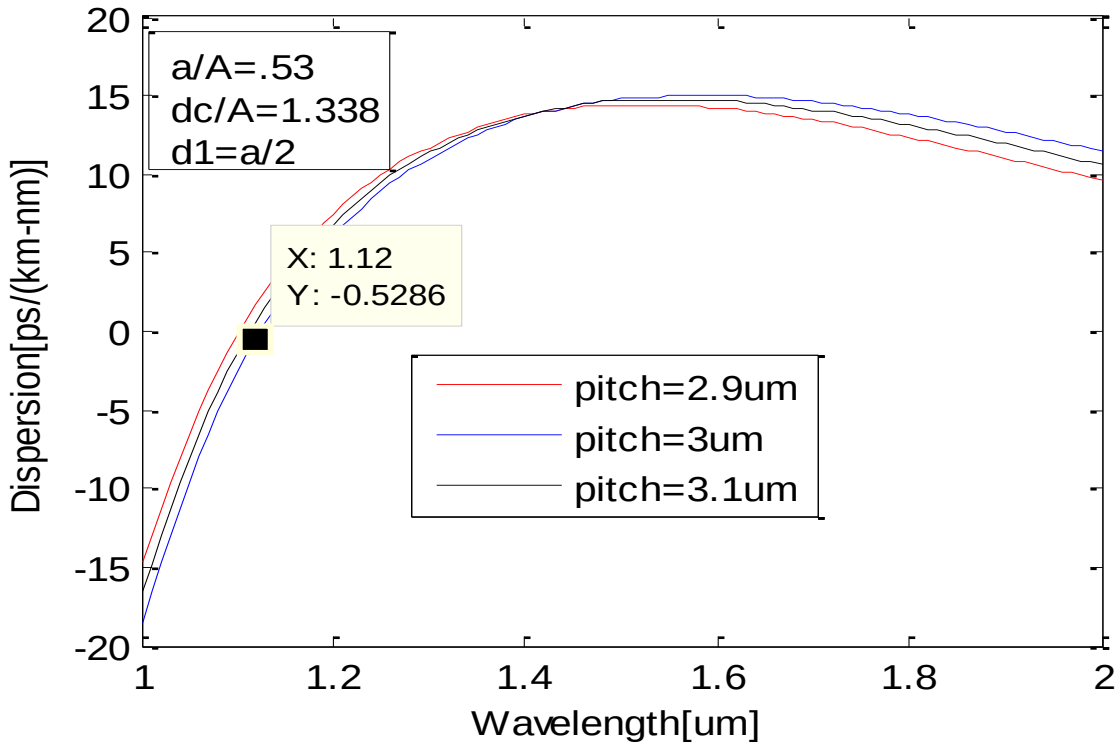

Fig 4.26 Dispersion profile of the proposed structure as a function of wavelength at 1% Doping concentration with the variation of pitch Λ.

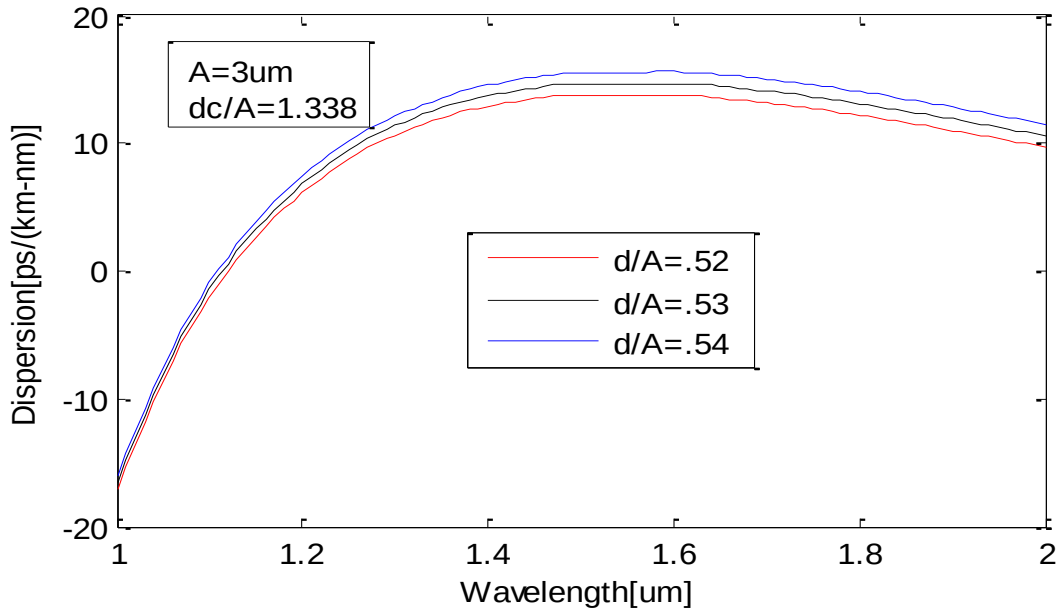

Fig 4.27 Dispersion profile of the proposed structure as a function of wavelength at 1% doping concentration With the variation of air hole diameter.

In fig 4.26 we show the total dispersion versus wavelength for different lattice constant. At d/Λ=.53 and dc/Λ=1.338, it can be seen here dispersion is negative value at operating wavelength 1.12µm. And for increasing the lattice constant dispersion profile shifts upward.

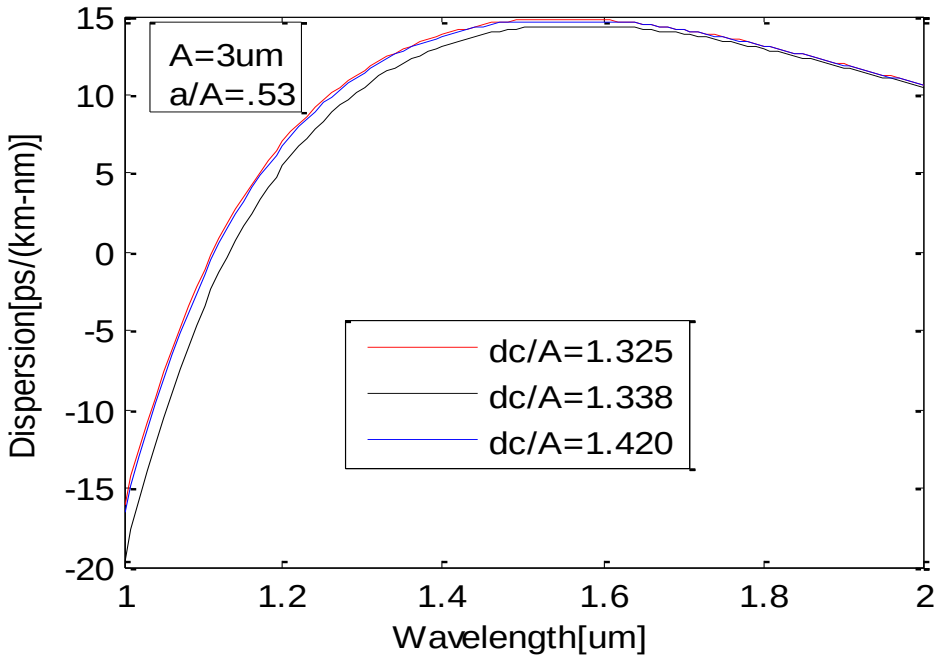

Fig 4.28 Dispersion profile of the proposed structure as function of wavelength at 1% doping concentration with the variation of side length of the square defected core.

In fig 4.27 we show the total dispersion versus wavelength for different air hole diameter. At Λ=3µm and dc/Λ=1.338, it can be seen here dispersion is very high at operating wavelength 1.55µm. And for increasing the air hole diameter dispersion profile shifts downward.

In fig 4.28 we found that the total dispersion versus wavelength for different side length of the square defected core also keeping nearest air hole diameter half of the diameter of other air hole. At Λ=3µm, a/Λ=.53 and d1=a/2, it can be seen here dispersion is very high at operating wavelength 1.55µm. And increasing the air hole diameter dispersion profile shifts upward.

4.4.2 Numerical Result of Nonlinear Properties

The empirical relation between the refractive index and the wavelength. The equation is used to determine the dispersion profile. The sellmeier equation for the silica glass is discussed in equation 4.1

Similarly the sellmeier equation for GeO_2 doped SiO_2 is given in equation 4.2

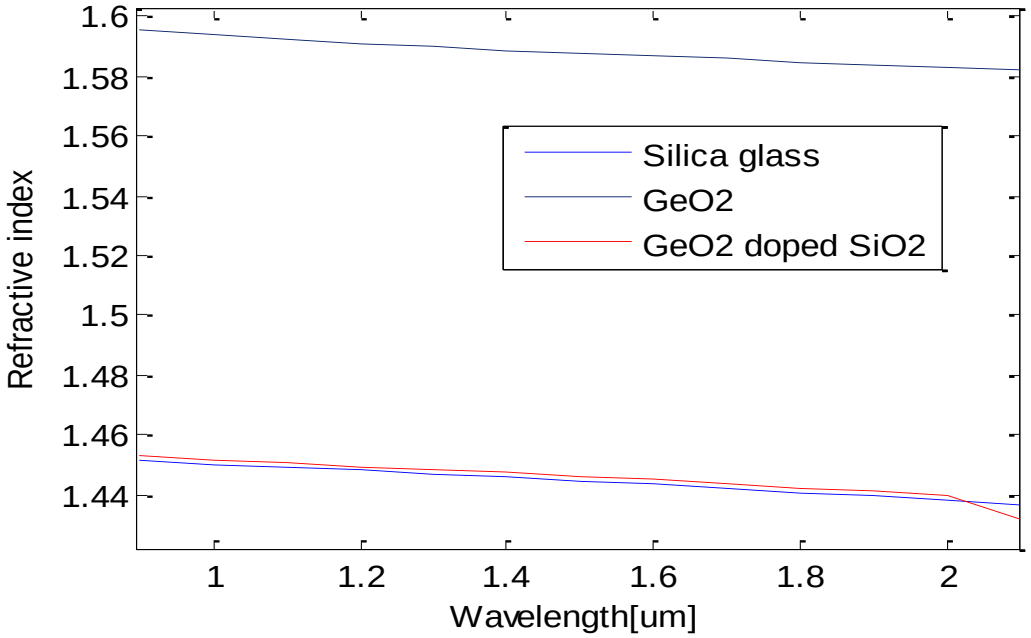

Fig 4.29 Refractive index of silica glass (blue line), GeO2 (black line) and GeO2 doped SiO2(red line) as a function of wavelength.

In fig 4.29, refractive index versus wavelength is plotted using the equation (4.1) and (4.2) for silica glass, GeO2 and GeO2 doped SiO2.

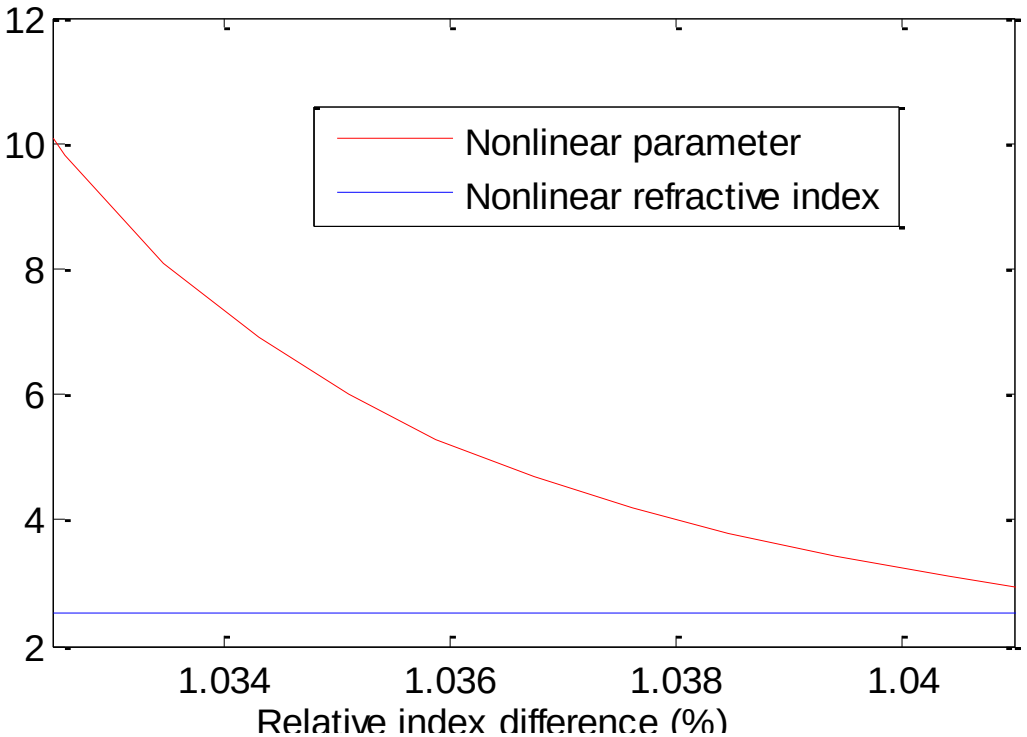

Fig 4.30 Nonlinear refractive index and nonlinear parameter as function of relative index difference.

In fig 4.30, nonlinear refractive index and nonlinear parameter is plotted as a function of relative index difference where we can see that as nonlinear parameter decreases nonlinear refractive index shows constant.

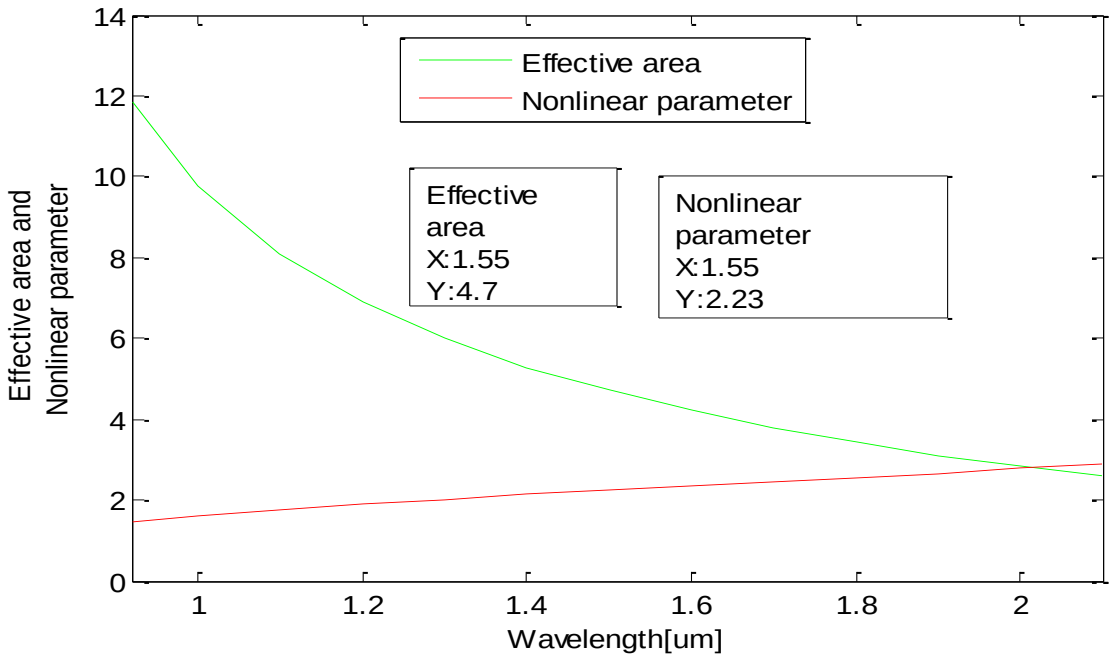

Fig 4.31 Nonlinear Parameter and Effective Mode area as a function of Wavelength.

In fig 4.31, effective mode area decreases with the wavelength. Since nonlinear parameter is increasing with the effective mode area, consequently nonlinear parameter increases with the increasing wavelength. At operating wavelength 1.55µm the effective mode area and non linearity parameter is 4.7μm^2 and 2.23$W^{-1}km^{-1}$.

CHAPTER 5

Conclusion

5.1 Summary

To summarize the 1st part of this thesis we have demonstrated an outstanding technique for controlling the chromatic dispersion in PCFs by introducing a GeO_2 doped defected SiO_2 square in the core of the proposed PCF model. Our proposed PCF model is significantly simpler than other structures proposed so far for controlling the chromatic dispersion and at the same time dispersion-flattened characteristics have been obtained in the S-band (1460nm-1530nm), C- band(1530-1565 nm) and L-band (1565nm-1625nm). Additionally our proposed PCF architecture shows low small effective mode area with high nonlinear gain. The main conclusion of this systematic approach is that with a modest number of design parameters we could fully-tune and optimize the chromatic dispersion properties of the PCF. The dispersion characteristics can be controlled by changing doping concentration, lattice constant, air hole diameter and square defected core side length. Our architecture is suitable for applications as a chromatic dispersion controller, dispersion compensator, or as candidate for nonlinear optical systems because of its small effective mode area. The proposed Dispersion Flattened Fiber (DFF) shows nearly zero dispersion (0.000187ps/km-nm) at operating wavelength (1.55um). It shows small effective mode area ($3.03um^2$) with high nonlinear gain ($67.23W^{-1}km^{-1}$) at operating wavelength. In the 2nd part of the thesis we proposed a different type structure to control the dispersion. Here we also demonstrated a PCF for which the dispersion will be flattened for large band. For this proposed structure dispersion shows negative for high doping concentration. But at low doping concentration the dispersion shows flatten line. So this structure is effective for lower doping concentration. Also nonlinear parameter can be minimized with the structure. At operating wavelength 1.55μm the dispersion is negative value and effective area $4.7\mu m^2$ with lower nonlinear parameter $2.23W^{-1}km^{-1}$.

5.2 Future work

Dispersion and nonlinear properties of an octagonal structure is going to be investigated shortly. We will calculate bending loss of the structure and compare it with our proposed structure,

Fundamental modes were focused more importantly than on other higher order modes while doing the optical characterization. Fundamental modes will have tighter confinement and less waveguide losses than the higher order modes. We are trying to investigate an analytic equation to predict the single mode behavior accurately.

Moreover theoretical study on novel nonlinear phenomenon such as Intrapulse Raman Scattering, Four Wave Mixing, Super continuum Generation, Temporal and Spectral Evolution, Second-Harmonic Generation and Third-Harmonic Generation is being carried
out.

A novel design of Dispersion Compensating Fiber (DCF) with ultra-high negative dispersion coefficient at operating wavelength is also in progress.

We have strong desire to investigate new medical application of PCF in near future.

References

[1] F.Zolla , "Foundations of Photonic Crystal Fibres" 2nd Edition,G.Renversez,A. Nicolet, B. Kuhlmey, S. Gueneau, D. felbacg, A. Argyros, S. Leon-Saval.

[2] J. C. Knight, "Photonic Crystal Fibers," Nature 424, 847-851 (2003).

[3] Russell,P.St.J., "Photonic Crystal Fibers" Science,Vol.299, PP. 358-362,jan.2003.

[4] C. Lin, "Photonic Crystal Fibers for Nonlinear Photonic Signal Processing and Biosensor Applications", Optical Internet, 2007 and 32ndAustralian Conference on Optical Fibre Technology, Joint International Conference on, pp. 1 - 4, 24-27 June 2007.

[5] Photonic crystals- Molding the flow of Light, 2nd Edition, John D. Joannopoulos, Steven G. Johnson, Joshua N. Winn, and Robert D. Meade.

[6] B. T. Kuhlmey, R. C. McPhedran, C. M. de Sterke, P. A. Robinson, G. Renversez, and D. Maystre, "Microstructured optical fibers: where‟s the edge?"Optics Express, vol. 10, pp.
1285-1290, Nov. 2002. http://www.opticsexpress.org/abstract.cfm?URI=OPEX-10-22-1285.

[7] N. A. Mortensen, J. R. Folkenberg, M. D. Nielsen, and K. P. Hansen, "Modal cutoff and the V parameter in photonic crystal fibers,"Optics Letters, vol. 28, pp. 1879-1881, Oct. 2003.

[8] J. C. Knight, J. Broeng, T. A. Birks, and P. St. J. Russell, "Photonic band gap guidance in optical fibers,"Science, vol. 282, pp. 1476-1478, Nov. 1998.

[9] W. H. Reeves, J. C. Knight, P. St. J. Russell, and P. J. Roberts, "Demonstration of ultra- flattened dispersion in photonic crystal fibers,"Optics Express, vol. 10, pp. 609-613, July
2002. http://www.opticsexpress.org/abstract.cfm?URI=OPEX-10-14-609.

[10] P. St. J. Russell, "Photonic-Crystal Fibers", J. Lightw. Technol., vol. 24, No. 12, Dec. 2006.

[11] P.St. J. Russell, "Designing photonic crystals", in Electron and Photon Confinement in

Semiconductor Nanostructures. Amsterdam, The Netherlands: IOS, pp. 79-103, 2003.

[12] Photonic Crystal For Communication Applications, Shanhui Fan*, ZhengWangb, David A.B. Millera,, P. R. Villeneuvec, H. A. Haus, and J. D. Joannopoulosc.

[13] J. K. Ranka, R. S. Windeler, and A. J. Stentz , "Visible continuum generation in air - silica microstructure optical fibers with anomalous dispersion at 800 nm", Opt. Lett.,vol. 25,
pp. 25-27, 2000.

[14] Photonic Crystal Fiber for Medical Applications, Feroza Begum and Yoshinori Namihira.
15] E. Coscelli, M.Sozzi, F. Poli, D. Passaro, A. Cucinotta, S. Selleri, R. Corradini, and R.
Marchelli, "Toward A Highly Specific DNA Biosensor: PNA-Modified Suspended-Core Photonic Crystal Fibers", *J. Quantum Electron.*, vol. 16, no. 4, pp. 967-972, Aug. 2010.

[16] A. S. Webb, F. Poletti, D. J. Richardson, and J. K. Sahu, "Suspended-core holey fiber for evanescent-field sensing",*Opt. Eng. Lett.*, vol. 46, no. 1, pp. 164-70, Jan. 2007.

[17] H. Ebendorff-Heidepriem and T. M. Monro, "Extrusion of complex preforms for micro-structured optical fibers", Opt. Exp., vol. 15, no. 23, pp. 15086-15092, 2007.

[18] Y. DeHazan, J. B. MacChesney, T. E. Stockert, D. J. Trevor, and R. S. Windeler, U.S. patent, 6,467,312 B1, Oct. 2002.

[19] R. T. Bise, and D. J. Trevor, "Sol-gel Derived Microstructured Fiber: Fabrication and

Characterization", Optical Fiber Conference, OWL6, Mar. 2005.

[20] M. N. Hossain, M. S. Alam, D. M. N. Hasan, and K. M. Mohsin, "A Highly Nonlinear Spiral Photonic Crystal Fiber for Tailoring two Zero Dispersion Wavelengths in the Visible
Region", Photonics Letter of Poland (PLP), vol. 2, no. 3, pp. 143-145, Sept. 2010.

[21] F.Zolla , **"**Foundations of Photonic Crystal Fibres**"** 2nd Edition,G.Renversez,A. Nicolet, B. Kuhlmey, S. Gueneau, D. felbacg, A. Argyros, S. Leon-Saval, Chapter-02, Page-782.

[22] P.Viale, S. Février, F. Gérôme, and H. Vilard, "Confinement Loss Computations in Photonic Crystal Fibres using a Novel Perfectly Matched Layer Design," Excerpt from the
Proceedings of the COMSOL Multiphysics User's Conference, Paris, 2005.

[23] COMSOL Multphysics, Version 4.3, 2012.

[24] M. Born and E. Wolf, Principles of Optics, 7th ed., Cambridge University Press, New York, 1999.

[25] I. H. Malitson, J. Opt. Soc. Am. 55, 1205 (1965).

[26] L. G. Cohen, C. Lin, and W. G. French, Electron. Lett. 15, 334 (1979).

[27] C. T. Chang, Electron. Lett. 15, 765 (1979); Appi. Opt. 18, 2516 (1979).

[28] L. G. Cohen, W. L. Mammel, and S. Lumish, Opt. Lett. 7, 183 (1982).

[29] S. J. Jang, L. G. Cohen, W. L. Mammel, and M. A. Shaifi, Bell Syst. Tech. J. 61, 385 (1982).

[30] V. A. Bhagavatula, M. S. Spotz, W. F. Love, and D. B. Keck, Electron. Lett. 19, 317 (1983).

[31] P. Bachamann, D. Leers, H. Wehr, D. V. Wiechert, J. A. van Steenwijk, D. L. A. Tjaden,
and E. R. Wehrhahn, J. Lightwave Technol. 4, 858 (1986).

[32] B. J. Ainslie and C. R. Day, J. Lightwave Technol. 4, 967 (1986).

[33] Fiber-Optic Communication Systems (Fourth Edition), Govind P. Agrawal

[34] G. P. Agrawal and M. J. Potasek, Opt. Lett. 11, 318 (1986).

[35] J. Zyskind, R. Barry, G. Pendock, M. Cahill, and J. Ranka, in Optical Fiber Telecom- munications, Vol. 4B, I. P. Kaminow and T. Li, Eds., Academic Press, Boston, 2002, Chap. 7.

[36] A. E. Willner and B. Hoanca, in Optical Fiber Telecommunications IV, Vol. 4B, I. P. Kaminow and T. Li, Eds., Academic Press, Boston, 2002, Chap. 14.

[37] M. Suzuki and N. Edagawa, J. Lightwave Technol. 21, 916 (2003).

[38] C. Lin, H. Kogelnik, and L. G. Cohen, Opt. Lett. 5, 476 (1980).

[39] A. J. Antos and D. K. Smith, J. Lightwave Technol. 12, 1739 (1994).

[40] K. Thyagarajan, R. K. Varshney, P. Palai, A. K. Ghatak, and I. C. Goyal, IEEE Photon. Technol. Lett. 8, 1510(1996).

[41] M. Onishi, T. Kashiwada, Y. Ishiguro, Y. Koyano, M. Nishimura, and H. Kanamori,Fiber Integ.Opt. 16,277(1997).

[42] J. Liu, Y. L. Lam, Y. C. Chan, Y. Zhou, and J. Yao, Fiber Integ. Opt. 18, 63 (1999).

[43] J.-L. Auguste, R. Jindal, J.-M. Blondy, M. Clapeau, J. Marcou, B. Dussardier, G. Monnom, D. B. Ostrowsky, B. P. Pal, and K. Thyagarajan, Electron. Lett. 36, 1689 (2000).

[44] L. Grüner-Nielsen, S. N. Knudsen, B. Edvold, T. Veng, D. Magnussen, C. C. Larsen,and H. Damsgaard, Opt. Fiber Technol. 6, 164 (2000).

[45] L. Grüner-Nielsen, M. Wandel, P. Kristensen, C J0rgensen, L. V. Jorgensen, B. Edvold,
B. Palsdottir, and D. Jakobsen, J. Lightwave Technol. 23, 3566
(2005)

[46] G. P. Agrawal, in Properties of Glass and Rare-Earth Doped Glasses for Optical Fibers,D. Hewak, Ed. (INSPEC, IEE, London, UK, 1998), pp. 17-21.

[47] M. Monerie and Y. Durteste, Electron. Lett. 23, 961 (1987).

[48] L. Prigent and J. P. Hamaide, IEEE Photon. Technol. Lett. 5, 1092 (1993).

[49] K. S. Kim, R. H. Stolen, W. A. Reed, and K. W. Quoi, Opt. Lett. 19, 257 (1994).

[50] Y. Namihira, A. Miyata, and N. Tanahashi, Electron. Lett. 30, 1171 (1994).
51] T. Kato, Y. Suetsugu, M. Takagi, E. Sasaoka, and M. Nishimura, Opt. Lett. 20, 988(1995).

[52] M. Artiglia, E. Ciaramella, and B. Sordo, Electron. Lett. 31, 1012 (1995).

[53] M. Artiglia, R. Caponi, F. Cisternino, C. Naddeo, and D. Roccato, Opt. Fiber Technol. 2,75 (1996).

[54] A. Boskovic, S. V. Chernikov, J. R. Taylor, L. Gruner-Nielsen, and O. A. Levring,Opt.Lett. 21, 1966 (1996).

[55] A. Fellegara,M. Artiglia, S. B. Andereasen, A.Melloni, F. P. Espunes, and M.Martinelli,Electron. Lett. 33, 1168 (1997).

[56] R. H. Stolen, W. A. Reed, K. S. Kim, and G. T. Harvey, J. Lightwave Technol. 16, 1006(1998)

[57] Nonlinear Fiber Optics (Fourth Edition), Govind P. Agrawal

[58] Kunimasa Saitoh, Nikolaos Florous, and Masanori Koshiba (2005), "Ultra-flattened chromatic dispersion controllability using a defected-core photonic crystal fiber with low confinement losses"

[59] Dispersion in GeO2-SiO2 glasses, James W. Fleming